

34 **Abstract**

35
36 Community-acquired urinary tract infection (UTI) is among the most common bacterial infections
37 observed in humans. Postmenopausal women are a rapidly growing and underserved
38 demographic group who are severely affected by rUTI with a >50% recurrence rate. In this
39 population, rUTI can persist for years, reducing quality of life and imposing a significant healthcare
40 burden. rUTI is most often treated by long-term antibiotic therapy, but development of antibiotic
41 resistance and allergy leave physicians with fewer treatment options. The female urobiome has
42 been identified as a key component of the urogenital environment. However, structural and
43 functional changes in the urobiome underlying rUTI susceptibility in postmenopausal women are
44 not well understood. Here, we used strictly curated, controlled cross-sectional human cohorts of
45 postmenopausal women, urobiome whole genome (shotgun) metagenomic sequencing (WGMS),
46 advanced urine culturing techniques, extensive biobanking of >900 patient-derived urinary
47 bacterial and fungal isolates, and mass spectrometry-based estrogen profiling to survey the
48 urobiome in rUTI patients during infection relapse and remission as well as healthy comparators
49 with no lifetime history of UTI. Our results suggest that a history of rUTI strongly shapes the
50 taxonomic and functional ecology of the urobiome. We also find a putative protective commensal
51 population, consisting of species known to convey protection against bacterial vaginosis such as
52 *Lactobacillus crispatus*, within the urobiome of women who do not experience UTI. Integration of
53 clinical metadata detected an almost exclusive enrichment of putative protective species
54 belonging to the genus, *Lactobacillus*, in women taking estrogen hormone therapy (EHT). We
55 further show that the urobiome taxonomic ecology is shaped by EHT, with strong enrichments of
56 putatively protective lactobacilli, such as *L. crispatus* and *L. vaginalis*. Integrating quantitative
57 metabolite profiling of urinary estrogens with WGMS, we observed robust associations between
58 urobiome taxa, such as *Bifidobacterium breve* and *L. crispatus*, and urinary estrogen conjugate
59 concentrations, suggesting that EHT strongly alters the taxonomic composition of the female
60 urobiome. We have further used functional metagenomic profiling and patient-derived isolate
61 phenotyping to identify microbial metabolic pathways, antimicrobial resistance genes (ARGs), and
62 clinically relevant antimicrobial resistance phenotypes enriched between disease-states. Our data
63 suggest distinct metabolic and ARG signatures of the urobiome associated with current rUTI
64 status and history. Taken together, our data suggests that rUTI history and estrogen use strongly
65 shape the functional and taxonomic composition of the urobiome in postmenopausal women.

66

67

68 **Introduction**

69 Urinary tract infection (UTI) is among the most common adult bacterial infections and imparts
70 particularly significant medical burden on women, with more than 50% of women suffering UTI in
71 their lifetime (Gaitonde et al., 2019; Jhang and Kuo, 2017). Historically, UTI has largely been
72 underprioritized in medical research due to low mortality rates and the effectiveness of available
73 antibiotics for most UTI episodes. However, UTI is a disease of disproportionate burden as age
74 is one of the strongest associated risk factors for UTI and the development of recurrent UTI (rUTI)
75 (Flores-Mireles et al., 2015). Indeed, it is estimated that approximately 50% of UTIs in
76 postmenopausal women develop into rUTI, which is clinically defined as ≥ 3 symptomatic UTIs in
77 12 months (Gaitonde et al., 2019; Malik et al., 2018b). rUTI can last for years, dramatically
78 decreasing quality of life and, if treatment is unsuccessful, can develop into life-threatening
79 urosepsis. Current therapeutic strategies mostly rely on the chronic use of antibiotics to achieve
80 urinary tract sterility (Flores-Mireles et al., 2015; Malik et al., 2018a; Neugent et al., 2020).
81 However, increasing rates of antibiotic refractory rUTI make this strategy unsustainable and
82 ultimately ineffective. For example, a recent prospective study of 86 postmenopausal women
83 observed resistance or allergy incidence rates of 76%, 56%, and 35% to the frontline antibiotics
84 trimethoprim-sulfamethoxazole (TMP-SMX), fluoroquinolones, and nitrofurantoin, respectively
85 (Malik et al., 2018a). These observations highlight the need for alternative therapeutic strategies
86 to combat the growing antibiotic resistance rates in the treatment of rUTI.

87 A promising source of therapeutic strategies for rUTI lies in modulating or restoring the urinary
88 microbiome, termed here the “urobiome” (Flores-Mireles et al., 2015; Stamm and Norrby, 2001).
89 Decades of medical dogma have largely assumed sterility of urine and the urinary tract. However,
90 a large body of work has robustly established the existence of a resident microbiome within the
91 human urinary tract (Brubaker and Wolfe, 2017; Hilt et al., 2014; Lewis et al., 2013; Price et al.,
92 2019; Siddiqui et al., 2011; Wolfe et al., 2012). Initial taxonomic analyses have associated
93 dysbiosis of the urobiome taxonomic composition to urinary incontinence, overactive bladder, and
94 bladder cancer (Bucevic Popovic et al., 2018; Karstens et al., 2016; Pearce et al., 2014). However,
95 fundamental knowledge of urobiome composition and function in postmenopausal women is
96 lacking. Studies surveying the microbial ecologies of the urobiome associated with UTI have
97 almost exclusively focused on premenopausal women or cohorts of mixed age (Barraud et al.,
98 2019; Brubaker and Wolfe, 2017; Hilt et al., 2014; Neugent et al., 2020; Price et al., 2019; Siddiqui
99 et al., 2011; Wolfe et al., 2012). As a result, the relationship between the urobiome and rUTI
100 susceptibility or treatment outcome is poorly understood in postmenopausal women. Interestingly
101 a 2021 report showed that pre and postmenopausal women displayed different core urinary

102 microbiota, providing strong rationale to characterize the postmenopausal urobiome in urogenital
103 disease (Ammitzboll et al., 2021).

104 Recently, the female urobiome has been reported to exhibit interconnection with the vaginal
105 microbiome (Thomas-White et al., 2018). For example, vaginal D(-)Lactate-producing lactobacilli,
106 known to protect the vagina from colonization by bacterial and fungal pathogens, have been
107 consistently observed in the female urobiome in multiple independent studies (Edwards et al.,
108 2019; Pearce et al., 2014). These observations beg the question of whether these known
109 protective vaginal species serve a similar protective role in the urobiome. Interestingly, a 2011
110 randomized clinical trial found a moderate reduction of rUTI incidence among women receiving
111 an intravaginal *L. crispatus* probiotic (Stapleton et al., 2011). While this study was performed in
112 premenopausal women and has yet to be validated in a larger clinical study, it does suggest that
113 lactobacilli may support urinary tract health. However, the niche-specific colonization and
114 metabolic needs of lactobacilli have not been assessed for this understudied ecosystem.

115 While numerous studies have used 16S rRNA amplicon sequencing to taxonomically profile the
116 microbial ecology of the human urobiome, no whole genome metagenomic sequencing (WGMS)
117 datasets have been generated to profile the genomic ecology of the urobiome in postmenopausal
118 women. Given the genomic diversity observed within and among taxonomic clades, metagenomic
119 information beyond 16S rRNA sequence enrichment is needed to assess the functional potential
120 of microbial communities (Quince et al., 2017). Whole-metagenome analysis of the urobiome is
121 required to identify the genes and metabolic pathways associated with urinary tract health, a
122 critical step towards the development of rationally designed probiotic therapies for rUTI. Here, we
123 present a WGMS survey of the urobiome of a strictly curated, cross-sectional cohort of
124 postmenopausal women separated into three groups defined by rUTI history and current UTI
125 status. Two of the cohort groups were curated to have recent rUTI history, differing only by current
126 infection status. The third cohort group consisted of postmenopausal women with no known
127 lifetime history of UTI. Our analysis has defined the urobiome ecology among the three cohorts
128 and has determined that the large-scale structure of the urobiome is not altered by rUTI history.
129 However, our taxonomic biomarker analysis using a Bayesian differential abundance model
130 identified significant species-level enrichments of gut bacteria and known uropathogens within the
131 urobiomes of women with rUTI history but no current UTI, suggesting that an imprint of past UTI
132 remains in the urobiome. We also observed a striking association between the use of estrogen
133 hormone therapy (EHT) and the presence of *L. crispatus* in the urobiome. Interestingly, we
134 observed differential enrichment of *Lactobacillus* spp. between patients using different EHT
135 modalities with strong *Lactobacillus* spp. enrichment among women using oral and patch EHT,

136 an observation which was not observed in patients using vaginal EHT. These findings mirror the
137 detected levels of excreted urinary estrogen conjugates in EHT(+) women. Functional analysis
138 revealed that the encoded metabolic potential is different between uropathogen-dominated and
139 commensal-dominated communities and that a history of rUTI dramatically alters the resistome
140 of the urinary microbiota with significant enrichments of beta-lactam, sulfonamide, and
141 aminoglycoside antimicrobial resistance genes associated with rUTI history. Taken together,
142 these results suggest that rUTI history and EHT shape the taxonomic and functional ecology of
143 the urobiome in postmenopausal women.

144

145 **Results**

146 **Cohort curation, metagenomic DNA preparation, and whole genome metagenomic dataset** 147 **generation**

148 Microbiome studies often observe high inter-sample variability, which can make interpretation
149 of ecological and associative analyses difficult (Fouts et al., 2012). With this in mind, we
150 implemented a strict set of exclusion criteria to guide patient recruitment and enrollment into the
151 study. Patients were excluded if they were premenopausal, seeking medical intervention for
152 complicated rUTI, diabetic, currently receiving chemotherapy, exhibiting renal insufficiency
153 (creatinine >1.5 mg/dL), using indwelling or intermittent catheters, had neurogenic bladder, or had
154 recent exposure to antibiotics within the last 4 weeks, unless an active infection was detected by
155 initial culture screening. rUTI often follows a cyclic pattern of infection relapse interrupted by
156 periods of remission (Figure 1A). To model this pattern of relapse and remission, the cohort of
157 postmenopausal women was stratified into three groups based on rUTI history. Group 1 served as
158 a healthy comparator and consisted of postmenopausal women with no lifetime history of
159 symptomatic UTI (No UTI History), group 2 consisted of postmenopausal women with a recent
160 history of rUTI but no active infection at the time of urine donation (rUTI Remission), and group 3
161 consisted of postmenopausal women with a history of rUTI and an active UTI at the time of urine
162 donation (rUTI Relapse) (Figure 1B). In total, 258 patients were recruited and screened for
163 enrollment candidacy through interview, clinical assessment, and electronic medical records.
164 29.8% of recruited patients passed the exclusion criteria and were enrolled. We determined that
165 25 patients per group was sufficient to balance a-priori sample size estimation (Figure S 1A, B)
166 with clinical feasibility and enrollment rates. Cohort demographic information is reported in Table
167 1.

168 Urine was collected via the clean catch midstream method after patients were educated about
169 the procedure for sample collection. It should be noted the clean-catch midstream urine samples

170 are representative of the urogenital microbiome (Karstens et al., 2018), which is inclusive of the
171 bladder, urethral, and, in some cases, vaginal microbiomes. Metagenomic DNA yields following
172 purification from cohort urine reflected the anticipated biomass of the urobiome in each group with
173 the highest DNA yields observed in women with active rUTI (rUTI Relapse). We collected a
174 median (\pm interquartile range) DNA mass of 62.1 ± 345.5 ng from No UTI History samples, 46.7
175 ± 198.2 ng from rUTI Remission samples, and 1822 ± 544 ng from rUTI Relapse samples (Figure
176 S 1C).

177 WGMS sequencing of human samples can suffer from a high degree of host contamination.
178 Previous reports of human contamination in WGMS sequencing of the urobiome range from 1-
179 99% of obtained reads (Moustafa et al., 2018; Quince et al., 2017). We therefore targeted 50
180 million reads per sample, balancing the higher cost of deep sequencing with the added advantage
181 of increased microbial sampling power. To remove host contamination, we mapped all reads
182 against the human genome reference (hg38) and collected unmapped reads, which represent all
183 non-human DNA sequenced. We observed an average of 67.57% host contamination within the
184 metagenomic sequencing data (Figure S 1E). After host removal, we generated a dataset with an
185 average of 2.6×10^7 non-human reads per sample.

186 To observe and measure potential contaminating background and environmental taxonomic
187 signals, a pure water sample was randomly inserted into the metagenomic DNA isolation
188 workflow, subjected to identical DNA isolation procedures, NGS sequencing, and taxonomically
189 analyzed with MetaPhlan2 (Segata et al., 2012). The majority of microbial reads observed in the
190 water control mapped to common nucleic acid purification kit and environmental contaminants
191 (Figure S 2A) (Salter et al., 2014). Except for known members of the human microbiome and
192 urobiome, these background taxa were censored from sample data when observed. We observed
193 a small relative abundance of taxa salient to the human urobiome in the water control, such as
194 *Pseudomonas*, *Escherichia*, *Klebsiella*, *Enterococcus*, *Staphylococcus*, and *Corynebacterium*.
195 These signals ranged from 0.0510%-11.5% of approximately 3 million mappable reads observed
196 in the water control.

197

198 **Validation of viable urobiome species through advanced urinary culture and WGMS hybrid** 199 **taxonomic profiling.**

200 To observe and validate the presence of living microbiota within the urobiomes sampled, we
201 coupled WGMS with advanced urine culture, a modification of the previously reported EQUIC
202 protocol (Price et al., 2016). Advanced culture of cohort urine both generated a detailed, species-
203 level taxonomic profile and validated the presence of living taxa detected within the urobiomes

204 sampled. Taxonomic profiling by WGMS revealed that the aggregate of the urobiomes sampled
205 was dominated by the kingdom, Bacteria, which represented 99.4% of the detected non-viral,
206 microbial taxa (Figure 1C). Consistent with what is known about the taxonomic composition of
207 urobiomes studied to date (Brubaker and Wolfe, 2017; Siddiqui et al., 2011), the detected
208 bacterial taxa across the entire cohort belong to 4 major phyla: Firmicutes (44.7%), Actinobacteria
209 (22.3%), Proteobacteria (20.6%), and Bacteroidetes (12%) (Figure 1C). Advanced urine culture
210 captured 93.9% of bacterial genera detected in WGMS with observed aggregate relative
211 abundance $\geq 5\%$ in any sample (Figure 1D). At the patient-level, advanced urine culturing was
212 able to validate the viability of an average of 74.5% of genera detected by WGMS (Figure S 2A).
213 The most frequent cultivable genera detected across all samples were *Lactobacillus*, *Escherichia*,
214 *Streptococcus*, *Bifidobacterium*, *Gardnerella*, *Klebsiella*, *Staphylococcus*, *Fingoldia*,
215 *Enterococcus*, and *Facklamia*. We cryo-preserved pure isolates from every cultivable species
216 detected through advanced urine culture and generated a large isolate biobank of 904 speciated
217 bacterial and fungal isolates, a first of its kind resource for the field.

218

219 **Analysis of urobiome ecology reveals similar ecological structure between women with** 220 **No lifetime UTI history and rUTI Remission.**

221 We next analyzed the genus and species-level taxonomic profiles and ecological structure
222 within the No UTI History, rUTI Remission and rUTI Relapse groups (Figure 2A, B, Figure S 3A).
223 Inspection of the rUTI Relapse group revealed urobiomes mainly dominated by single bacterial
224 uropathogens with little detected abundance of *Eukarya* and *Archaea* (Figure 2B, Figure S 3A).
225 The most prevalent uropathogen detected in our analysis was *Escherichia coli* (15/25, 60%), a
226 species known to be the major uropathogen among most types of UTI (Flores-Mireles et al.,
227 2015). Along with *E. coli*, our analysis also detected known uropathogens, *Klebsiella pneumoniae*
228 (2/25, 8%), *Enterococcus faecalis* (1/25, 4%), and *Streptococcus agalactiae* (1/25, 4%). We also
229 observed a low relative abundance of fungal species within the rUTI Relapse urobiomes including
230 *Candida glabrata* and *Malassezia globosa*. Similarly low amounts of Archaeal taxa were
231 detected, such as, *Methanobrevibacter spp* (Figure S 3A). Interestingly, we observed viral taxa
232 present within the urobiomes of the rUTI Relapse cohort. The most observed virus was JC
233 polyomavirus (4/25 16%) but Human herpes virus 4 (1/25 4%) and Enterobacteria phage Iike (1/25
234 4%) were also detected (Figure S 3B).

235 The most frequently observed bacterial species in urobiomes of women without active infection
236 (No UTI History and rUTI Remission) belonged to the genera *Lactobacillus*, *Bifidobacterium*,
237 *Gardnerella*, *Streptococcus*, *Staphylococcus*, and *Actinobaculum* (Figure 2 A, B). A subset of

238 these samples (54%) were dominated by one taxon while others were diverse and exhibited no
239 single dominant taxon. We observed 13 patients (24%) in the No UTI History and rUTI Remission
240 groups with a >50% relative abundance of various *Lactobacillus spp.*, including *L. crispatus*, *L.*
241 *iners*, and *L. gasseri* (Figure 2B). Interestingly, we also observed a subset of urobiomes in the No
242 UTI History and rUTI Remission groups dominated by *Bifidobacterium spp.*, such as *B. breve*, *B.*
243 *dentium*, and *B. longum*, as well as *Gardnerella vaginalis* (Figure 2B). Fungal and archaeal
244 species were also observed in low abundance (0-8.8% relative abundance) in the No UTI History
245 and rUTI Remission urobiomes (Figure S 3A). Three species of *Candida*, including *C. albicans*,
246 *C. glabrata*, and *C. dubliniensis* were detected. Other fungal taxa observed include *Malassezia*
247 *globosa*, *Naumovozya spp.*, and *Eremothecium spp.* Observed archaeal species within the No
248 UTI History and rUTI Remission urobiomes included *Methanosphaera stadtmanae* and
249 *Methanobrevibacter spp.* Viral taxa were more frequently observed in the No UTI history and rUTI
250 Remission groups as compared to the rUTI Relapse group (Figure S 3B). The most observed
251 viral taxa in the No UTI history and rUTI Remission groups were JC polyomavirus, BK
252 polyomavirus, and Merkel cell polyomavirus (Figure S 3B).

253 To model the urobiome ecological structure within the three groups, we calculated alpha-
254 diversity indices including the observed taxa count, Shannon, Simpson, Chao 1, and ACE indices
255 (Thomas-White et al., 2017). Our analysis found that women in the No UTI History and rUTI
256 Remission groups had similarly diverse urobiomes across different alpha diversity indices (Figure
257 2C, D, Figure S 4 A, B, C). These data suggest that if there are ecological differences in the
258 urobiomes of postmenopausal women who are susceptible to rUTI (rUTI Remission) versus those
259 who are not (No UTI History), they are not reflected in alpha diversity metrics. The rUTI Relapse
260 group exhibited significantly lower alpha diversity indices as compared to the rUTI Remission
261 cohort, an observation that is likely attributed to uropathogen niche dominance during active
262 infection (Figure 2C, D, Figure S 4 A, B, C).

263 To assess large-scale taxonomic signatures associated with rUTI history and infection status,
264 we used double principal coordinate analysis (DPCoA), a beta-diversity ordination method which
265 allows for dimensionality reduction through relative abundance weighted phylogenetic distance
266 calculation between samples (Pavoine et al., 2004). Visualization of the first two PCoAs applying
267 weighted DPCoA to the aggregate dataset of detected species in the cohort revealed clustering
268 of the urobiomes of the rUTI Relapse group along a vector defined by the enrichment of *E. coli*
269 and were ecologically distinct from the urobiomes of the No UTI History and rUTI Remission
270 groups. The No UTI History and rUTI Remission groups exhibited relatively similar clustering
271 patterns in the first two PCoAs (Figure 2E) and many of these women clustered along opposing

272 vectors defined by the enrichment of either *L. crispatus* or *G. vaginalis*, which are associated with
273 a healthy vaginal microbiome or bacterial vaginosis, respectively (Ravel and Brotman, 2016;
274 Ravel et al., 2011). This similar clustering pattern between the No UTI history and rUTI Remission
275 cohorts suggests that a history of rUTI does not significantly alter the large-scale taxonomic
276 structure of the urobiome in postmenopausal women. However, the clustering of the No UTI
277 History and rUTI Remission urobiomes along the vectors defined by *L. crispatus* or *G. vaginalis*
278 supports an association between the urinary and vaginal microbiomes as previously reported
279 (Thomas-White et al., 2018).

280

281 **Taxonomic co-occurrence analysis identifies three non-interacting microbial clusters** 282 **within the urobiome.**

283 Microbial communities can harbor intricate interactions between member taxa (Alteri et al.,
284 2015; Keogh et al., 2016). Exceedingly little is known about interactions and co-occurrence of
285 bacterial species within the urobiome. We used the CCREPE pipeline to compute pairwise
286 associations and a compositionally corrected statistical association assessment between genera
287 detected within the cohort urobiomes (<https://huttenhower.sph.harvard.edu/ccrepe/>) (Figure 2F).
288 This analysis identified 2025 non-zero taxa correlations that were further filtered to 87 statistically
289 significant associations ($P < 0.05$) (Figure 2F). After multiple hypothesis testing correction, a total
290 of 17 unique microbial associations exhibited robust statistical significance ($Q < 0.05$) (Figure 2F).
291 Network visualization of significant associations ($P < 0.05$) revealed three non-interacting microbial
292 clusters (Figure 2G). Cluster 1 member taxa were all known members of the human gut
293 microbiome (Human Microbiome Project, 2012). Cluster 2 exhibited the largest member set and
294 diversity and captured associations between genera known to inhabit the urobiome but whose
295 association has not yet been reported. Cluster 2 member genera, such as *Peptoniphilus* and
296 *Fingoldia*, have been reproducibly observed in the human urobiome in multiple, independent
297 studies (Anglim et al., 2021; Thomas-White et al., 2017). Interestingly, Cluster 2 grouped strongly
298 around the genus *Peptoniphilus*, a member of the vaginal microbiome that is known to be
299 associated with dysbiosis (Diop et al., 2019). Cluster 3 was identified as a pairwise interaction
300 between the genera *Gardnerella* and *Atopobium*, two taxa that have been previously associated
301 in vaginal dysbiosis and bacterial vaginosis (Bradshaw et al., 2006; Hardy et al., 2016; Hardy et
302 al., 2015). Taken together, these data suggest that taxonomic signatures within the urobiome of
303 postmenopausal women may follow patterns of co-occurrence, an observation which merits
304 further mechanistic study.

305

306 **Taxonomic biomarker analysis reveals that rUTI history alters the species-level taxonomic**
307 **signature of the urobiome.**

308 rUTI follows a cyclic pattern of active infection followed by periods of no infection or remission
309 (Figure 1A). We and others have observed that the taxonomic profiles of the urobiomes of
310 individuals with UTI are significantly different than healthy individuals (Figure 2 A,B) (Flores-
311 Mireles et al., 2015). Taxonomic remodeling associated with infection has also been shown to
312 significantly alter the microbiome in other niches throughout the human body. Interestingly,
313 taxonomic remodeling of the gut microbiome associated with antibiotic use is the strongest risk
314 factor associated with the development of *Clostridium difficile* infection (Theriot et al., 2014). To
315 test the hypothesis that rUTI history alters the underlying urobiome, we performed genus and
316 species-level differential taxonomic enrichment analysis between the urobiomes of the No UTI
317 History and the rUTI Remission patients. We employed the linear discriminant analysis of effect
318 size (LEfSe) to incorporate an extensively employed non-parametric assessment of differential
319 taxonomic abundance (Segata et al., 2011). We also employed the Bayesian microbial differential
320 abundance (BMDA) model that can account for common characteristics that complicate
321 differential analysis of microbiome data, such as data sparsity (zero inflation), over-dispersion,
322 and uneven sampling depth (Li et al., 2019). Differentially enriched taxa detected by these
323 analyses may serve as candidate taxonomic biomarkers for urobiome dysbiosis and possibly rUTI
324 susceptibility. LEfSe detected no differentially abundant taxa between the No UTI History and
325 rUTI Remission groups. However, using the BMDA model, we detected multiple differentially
326 abundant taxa between No UTI History and rUTI Remission groups. BMDA detected two genera,
327 *Aerococcus* ($\log_{10}(\text{Posterior Effect Size}) = 0.70$, PPI = 0.97) and *Lactobacillus* ($\log_{10}(\text{Posterior}$
328 $\text{Effect Size}) = 0.52$, PPI = 0.96), as well as two species of lactobacilli, *L. vaginalis* ($\log_{10}(\text{Posterior}$
329 $\text{Effect Size}) = 7.66$, PPI = 1) and *L. crispatus* ($\log_{10}(\text{Posterior Effect Size}) = 1.36$, PPI = 1), as
330 significantly enriched in the No UTI History group compared to the rUTI Remission group (Figure
331 3A, B). At the genus-level, *Klebsiella*, *Gemella*, *Bacteroides*, *Clostridiales Family XIII Incertae*
332 *Sedis unclassified*, *Eggerthella*, and *Escherichia* were among the most significantly enriched in
333 the rUTI Remission group compared to the No UTI History group. Fifteen species were identified
334 as significantly enriched in the rUTI Remission group, including *Ureaplasma parvum*, *Bacteroides*
335 *uniformis*, *E. faecalis*, *Staphylococcus hominis*, and *Staphylococcus epidermidis* (Figure 3B).
336 Many taxa enriched in the rUTI Remission group are primarily known to be native to the human
337 gut microbiome and not the female urobiome or vaginal microbiome (Figure 3 A, B). Taken
338 together, these results suggest that rUTI history may leave an imprint on urobiome composition
339 that may be missed by common ecological indices (alpha or beta diversity) and traditional

340 differential abundance pipelines that do not consider the sparsity, over-dispersion and uneven
341 sampling that is common in low biomass microbiomes like the urobiome (Karstens et al., 2018).

342

343 **Estrogen hormone therapy and urinary estrogen concentration is associated with** 344 ***Lactobacillus* abundance in the urobiome of postmenopausal women**

345 Given that many of the urobiomes of women without active rUTI were dominated by species of
346 lactobacilli (26%, 13/50) (Figure 2 A, B), we sought to further characterize this taxonomic
347 enrichment in the No UTI History and rUTI Remission groups. We screened the cohort-associated
348 clinical metadata for any variables associated with *Lactobacillus* abundance. Interestingly, we
349 found that estrogen hormone therapy (EHT) was strongly associated with the presence of
350 *Lactobacillus* in the urobiome (Figure 4 A, B, C). Ecological modeling revealed that the urobiomes
351 of EHT(+) women were significantly less diverse than those of EHT(-) women and tended to be
352 dominated by a single species belonging to the genus, *Lactobacillus* (Figure 4 D, E, F). To
353 determine how EHT shapes the taxonomic profile of the urobiome, we performed differential
354 taxonomic enrichment analysis using LEfSe and BMDA. The LEfSe identified the enrichment of
355 the species *L. crispatus* in patients using EHT and the enrichment of the genus, *Streptococcus*,
356 in patients not using EHT (*L. crispatus* LDA=5.1, $P=0.0185$; *Streptococcus* LDA=4.8, $P=0.0081$)
357 (Figure 4 G). Differential enrichment analysis using BMDA captured a similar result but was able
358 to further resolve species-level differential enrichment (Figure 4 H). *L. crispatus* and *L. vaginalis*,
359 were significantly enriched in the urobiomes of EHT(+) women (*L. crispatus* \log_{10} (Posterior Effect
360 Size) = 13.5, PPI=1; *L. vaginalis* \log_{10} (Posterior Effect Size) = 8.5, PPI=1). Interestingly, BMDA
361 detected species-level enrichment of the *Streptococcus mitis/oralis/pneumoniae* (*S. m/o/p*) group,
362 *Streptococcus infantis*, and *Atopobium vaginae* within the urobiomes of EHT(-) women (*S. m/o/p*
363 \log_{10} (Posterior Effect Size)= 8.8, PPI=1; *S. infantis* \log_{10} (Posterior Effect Size)= 9.2, PPI=1; *A.*
364 *vaginae* \log_{10} (Posterior Effect Size)= 13.9, PPI=1) (Figure 4H). Taken together, these data
365 suggest a strong association between EHT use and urobiome dominance by *Lactobacillus*
366 species known to convey protection against bacterial pathogens (Edwards et al., 2019).

367 EHT can be administered via multiple modalities including oral supplementation, transdermal
368 patch, and topical vaginal cream (Lobo, 2017). Using the cohort-associated clinical metadata, we
369 stratified patients based on EHT modality. Interestingly, we observed that women using oral and
370 patch EHT exhibited significant urobiome enrichment of *Lactobacillus*. However, urobiome
371 *Lactobacillus* enrichment varied widely in women using vaginal EHT (vEHT) and was not
372 significantly different from EHT(-) women (Figure 5A). We hypothesized that the vEHT may differ
373 from oral and transdermal patch in composition, metabolism, or dosage. We therefore used a

374 modified version of previously published targeted liquid-chromatography mass spectrometry (LC-
375 MS) methods for the measurement of urinary estrogens to quantify excreted urinary estrogen
376 conjugates of women in the No UTI History and rUTI Remission groups (van der Berg et al.,
377 2020). Limiting our analysis to the known major excreted sulfate and glucuronide conjugates of
378 estrone (E1) and 17 β -estradiol (E2), we observed significantly higher urinary E1 and E2
379 conjugate abundance, both sulfates and glucuronides, in women using oral EHT, an observation
380 concordant with observed urinary *Lactobacillus* abundance (Figure 5 B, C, D Figure S 6 A, B, C,
381 D). Women using patch EHT also exhibited high urinary *Lactobacillus* abundance and we
382 observed a significant enrichment of E1-sulfate in patch EHT(+) women compared to EHT(-)
383 women (Figure S 5C). Consistent with urinary *Lactobacillus* abundance, we observed no
384 statistically significant difference in urinary estrogen conjugate concentrations between vEHT(+)
385 women and EHT(-) women (Figure 4 A, B, C, D Figure S 5 A, B, C, D).

386 We further sought to determine if rUTI history differentially affected the EHT-associated
387 taxonomic signature by dichotomizing patients by No UTI History and rUTI Remission group
388 membership. We then performed exploratory correlation analysis of creatinine-normalized
389 estrogen metabolite concentrations and the species-level taxonomic profile. Multiple studies have
390 assessed association between urinary and vaginal *Lactobacillus* abundance and host estrogen
391 status with varying conclusions (Anglim et al., 2021; Thomas-White et al., 2020). However, it
392 remains unknown if urinary *Lactobacillus* abundance is directly correlated with host systemic or
393 excreted estrogen concentration. Interestingly, we observed a striking difference in the estrogen-
394 associated taxonomic profile between the No UTI History and rUTI Remission groups (Figure 5
395 E, F). We observed strong correlations between urinary E1 and E2 conjugates and three species
396 of *Lactobacillus*, *L. crispatus*, *L. iners*, and *L. gasseri*, in the No UTI History group, correlations
397 which were not detected in the rUTI Remission group (Figure 5 E, F Figure S 5 E, F). Interestingly,
398 *Bifidobacterium breve*, an *Actinobacterium* often used in probiotics and associated with colon
399 health, exhibited the strongest positive association across estrogen conjugates in the No UTI
400 History group (Figure 5 E, G). This observation was again absent in the urobiomes of the rUTI
401 Remission group. We observed one species, *Anaerococcus prevotii*, which was consistently and
402 significantly negatively associated with urinary estrogens in the No UTI History group (Figure 5 E,
403 Figure S 5 E). Interestingly, fewer and distinct taxa correlated with estrogen conjugates in the
404 rUTI Remission group (Figure 5 F, Figure S 5F). It should be noted that most EHT(+) women in
405 the rUTI Remission group used vEHT, which was not found to be associated with urobiome
406 *Lactobacillus* abundance (Figure 5 A). Taken together, these data demonstrate a direct
407 correlation between excreted urinary estrogen conjugate concentration and urobiome abundance

408 of known protective urogenital lactobacilli, such as *L. crispatus*. The data indicate that the
409 correlation between specific estrogen metabolites and urobiome is dependent on previous rUTI
410 history, suggesting that both rUTI history and estrogen shape the taxonomic ecology of the
411 urobiome.

412

413 **Functional profiling reveals significant differences in the metabolic potential of cohort** 414 **urobiomes.**

415 The genes encoded within a microbial community define the phenotypic capabilities of its
416 members. We used the HUMAnN (v2.0) pipeline to profile the metabolic potential encoded within
417 the cohort urobiomes (Franzosa et al., 2018). We sought to determine if rUTI history leaves a
418 detectable imprint on the functional metabolic potential of the urobiome. We further sought to
419 define the metabolic potential of the urobiomes of women who do not experience UTIs compared
420 to the rUTI Relapse group. Principal component analysis (PCA) performed on the relative
421 abundance of detected encoded metabolic pathways in the three groups identified discriminating
422 clusters that separated many of the rUTI Relapse urobiomes from the rUTI Remission and No
423 UTI History urobiomes in the first two principal components (PCs) (35.39% cumulative variance
424 explained in PC1 and 2) (Figure 6A). These results were consistent with those observed in the
425 taxonomic beta-diversity analysis (Figure 2 E). Analysis of the PCA loadings within the first two
426 PCs found that the rUTI Relapse group ordinated along vectors defined by the enrichment of
427 lipopolysaccharide (LPS) biosynthesis ($n=4$ pathways), demethylmenaquinol-8 biosynthesis,
428 Fucose and Mannose degradation, D-galacturonate degradation, Sucrose degradation, and the
429 TCA cycle (Figure 6B). Interestingly, rUTI Remission and No UTI History groups, which were not
430 discriminated in the first two PCs, tended to ordinate along vectors defined by the genetic
431 enrichment of nucleotide biosynthesis pathways ($n=8$ pathways), L-lysine biosynthesis II, S-
432 adenosyl methionine (SAM) biosynthesis, and UDP-N-acetyl-glucosamine biosynthesis (Figure
433 6B). These data suggest that the large-scale genetic potential of the urobiome is relatively similar
434 between rUTI Remission and No UTI History groups but is dramatically altered during active rUTI.

435 Because dimensional reduction techniques tend to lose fine-scale discriminating features, we
436 next sought to identify unique metabolic enrichments using pairwise comparisons. We used the
437 LEfSe microbial biomarker identification pipeline to identify discriminatory metabolic pathway
438 enrichments between the No UTI History group and the rUTI Remission or rUTI Relapse groups
439 (Segata et al., 2011). First, we tested the hypothesis that rUTI history imparts functional changes
440 on the urobiomes of PM women by comparing the No UTI History and rUTI Remission groups.
441 The analysis identified 49 metabolic pathways differentially enriched between the No UTI History

442 and rUTI Remission groups with an FDR-corrected $P < 0.05$ and LDA > 2 (Figure 6C). Forty-five
443 discriminatory metabolic pathways were significantly enriched in the rUTI Remission urobiomes
444 and 4 metabolic pathways significantly enriched in the No UTI History urobiomes. The top 40
445 differentially enriched pathways discriminating No UTI History from rUTI Remission urobiomes
446 primarily belonged to carbohydrate metabolism ($n=14$), electron carrier biosynthesis ($n=8$), amino
447 acid metabolism ($n=5$), cell envelope building block biosynthesis ($n=4$), vitamin and cofactor
448 biosynthesis ($n=4$), and polysaccharide degradation ($n=3$) (Figure 6C). While most of the
449 discriminatory carbohydrate metabolic pathways were enriched in the rUTI Remission urobiomes
450 (13/14, 92.9%), we observed an enrichment of D-galactose degradation (Leloir pathway) in the
451 urobiomes of the No UTI History group (LDA=3.06, $P=0.028$). Interestingly, we observed a strong
452 enrichment of electron carrier biosynthesis pathways in the rUTI Remission urobiomes.
453 Biosynthetic pathways for ubiquinol 7, 8, 9, and 10 as well as menaquinol 6, 9 and 10 and
454 demethylmenaquinol 9 were strongly enriched in the rUTI Remission urobiomes (Figure 6C). L-
455 lysine biosynthesis, L-threonine biosynthesis, and L-tryptophan degradation were observed to be
456 enriched in the No UTI History urobiomes, while L-ornithine biosynthesis and L-arginine
457 degradation were found to be enriched in the rUTI Remission urobiomes. The remaining
458 discriminating metabolic pathways were enriched in the rUTI Remission urobiomes and included
459 cell envelope biosynthesis (e.g. LPS biosynthesis), vitamin metabolism (e.g. coenzyme A
460 biosynthesis), polysaccharide degradation (e.g. 4-deoxy L-threo hex-4-enopyranuronate
461 degradation), cinnamate and hydroxy cinnamate degradation, and ppGpp biosynthesis (Figure
462 6C). These data suggest that the functional metabolic landscape of the urobiome may be
463 significantly altered by rUTI history.

464 We next performed pairwise differential pathway enrichment analysis between the No UTI
465 History and rUTI Relapse groups to test the hypothesis that the functional potential of the
466 urobiome is altering during rUTI. This analysis identified 183 discriminatory metabolic pathways
467 differentially enriched between the No UTI History and rUTI Relapse groups with a P -value less
468 than 0.05 and LDA > 2 (Figure 6D). We observed 50 and 133 metabolic pathways significantly
469 enriched in No UTI History and Relapsed rUTI groups, respectively (Figure 6D). In line with the
470 taxonomic enrichment of Gram-negative species, we observed a strong enrichment of
471 biosynthetic pathways for lipopolysaccharide (LPS) within the rUTI Relapse cohort. The top 40
472 most discriminating pathways mainly represent carbohydrate ($n=13$), nucleotide ($n=9$), and amino
473 acid metabolism ($n=6$), as well as cell envelope biosynthesis ($n=5$) (Figure 6D). We also observed
474 a striking enrichment of diverse carbohydrate degradation and central carbon metabolism
475 pathways, including rhamnose, fucose, glyoxylate, and fructuronate degradation in rUTI Relapse

476 urobiomes (Figure 3D). This was coupled with a significant enrichment of TCA cycle metabolism,
477 particularly 2-oxoglutarate decarboxylase and ferredoxin, within the urobiomes of the rUTI
478 relapse cohort (Figure 3D). Interestingly, only four metabolic pathways involved in carbohydrate
479 metabolism, including glycolysis from glucose and glucose 6-phosphate (G6P), pyruvate
480 fermentation, and N-acetyl glucosamine biosynthesis, were among the top 40 differentially
481 enriched within the No UTI History urobiomes (Figure 3D). There was a strong enrichment of
482 nucleic acid biosynthesis pathways among the urobiomes of the No UTI History group while the
483 Relapsed rUTI group was strongly enriched for nucleic acid degradation pathways (Figure 6D).
484 Differentially enriched amino acid metabolism pathways included strong enrichments for L-lysine,
485 L-threonine, and L-isoleucine biosynthesis in the No UTI History group as well as L-phenylalanine
486 biosynthesis in the rUTI Relapse group (Figure 3D). These results suggest that the metabolic
487 potential of the urobiome is significantly altered during active rUTI with the urobiomes of the rUTI
488 Relapse group displaying the ability to utilize a more diverse nutrient set than the urobiome of
489 women who do not experience UTI.

490

491 **History of rUTI alters the resistance genotype and phenotype of the urobiome**

492 Antibiotic therapy is currently the most prescribed treatment for the management of rUTI.
493 However, resistance to front-line antibiotic regimens, such as TMP-SMX, fluoroquinolones, and
494 nitrofurantoin, is becoming a significant barrier to the successful treatment of rUTI (Malik et al.,
495 2018a). We used the GROOT resistome analysis pipeline to generate a detailed profile of the
496 antimicrobial resistance genes (ARGs) encoded within the urobiomes of the women in each study
497 group (Rowe and Winn, 2018). This analysis detected an aggregated total of 55 distinguishable
498 ARGs distributed among all three patient groups. We observed significantly more ARG's present
499 in the urobiomes of the rUTI Remission ($P=0.0455$) and rUTI Relapse ($P=0.0302$) groups as
500 compared to the No UTI History urobiomes (Figure 7A). Interestingly, there was no significant
501 difference in ARG count between rUTI Relapse and rUTI Remission urobiomes, suggesting that
502 the urobiomes of women with rUTI history, independent of current rUTI status, harbor more ARGs
503 than the urobiomes of women with No UTI History. These results suggest that a history of rUTI
504 leaves an imprint on the underlying resistome of the urinary microbiota in postmenopausal
505 women.

506 To directly assess ARG enrichments associated with rUTI history, we performed differential
507 enrichment analysis using a Bayesian model of proportional enrichment with an objective Jeffrey's
508 prior (Jeffreys, 1946). This analysis identified the TEM β -lactamase family, the sulfonamide
509 resistance genes *sul1* and *sul2*, and the *straA* aminoglycoside 3'-phosphotransferase as

510 significantly differentially enriched in the rUTI Relapse group. We further observed significant
511 enrichments of the aminoglycoside 3'-phosphotransferase genes, *aph(3')-III* and *aph(3')-Ia*, the
512 macrolide resistance gene, *ermB*, the β -lactam resistance gene *mecA*, and the aminoglycoside
513 O-nucleotidyltransferase gene, *ant(6)-Ia*, in the urobiomes of the rUTI Remission group (Figure
514 7B). Interestingly, no ARGs were found to be statistically enriched in the No UTI History group,
515 further suggesting that rUTI history is associated with an accumulation of ARGs within the
516 urobiome. Taken together, these data suggest that urobiomes of women with active rUTI
517 frequently harbor ARGs conferring resistance to the commonly used antibiotic classes: β -lactams,
518 sulfanomides, and aminoglycosides. Of note, the urobiomes of the rUTI Relapse group were
519 found to be significantly enriched for *sul1* and *sul2*, which confer resistance to sulfanomides such
520 as sulfamethoxazole, one of the most common prescribed antibiotic therapies for rUTI (Köljalg et
521 al., 2009).

522 Genotypic assessments of ARG presence in metagenomes can only predict the phenotype of
523 a microbe or set of microbes belonging to the sampled population (Quince et al., 2017). Given
524 the observed enrichment of ARGs within rUTI Relapse urobiomes, we sought to phenotypically
525 assess the resistance characteristics, by disc diffusion, of 22 unique bacterial uropathogens
526 isolated from 22 women of the actively infected rUTI Relapse group. The bacterial isolates
527 generated from these women represented many known uropathogens including *E. coli* (UPEC)
528 ($n=15$), *K. pneumoniae* ($n=2$), *Klebsiella oxytoca* ($n=1$), *Streptococcus anginosus* ($n=2$), *S.*
529 *agalactiae* ($n=1$), *E. faecalis* ($n=1$), and *S. epidermidis* ($n=1$). We observed 15 isolates exhibiting
530 either complete or intermediate resistance to the penicillin β -lactam, Ampicillin (Amp), and 4
531 isolates exhibiting either complete or intermediate resistance to the cephalosporin β -lactam
532 Cefixime (Cfx) (Figure 7C). Of the isolates exhibiting β -lactam resistance phenotypes, 80%
533 (12/15) and 50% (2/4) were isolated from urobiomes for which WGMS resistome profiling detected
534 ARGs conferring resistance to Amp and CFX, respectively (Figure 7C). We observed that 50% of
535 isolates exhibiting resistance to Trimethoprim/Sulfamethoxazole (TMP/SMX) were isolated from
536 urobiomes for which WGMS resistome profiling detected the presence of the ARGs *Sul I/II* and
537 *DrfA1* (Figure 7C). Aminoglycoside resistance to Gentamycin (Gen), Kanamycin (Kan), Amikacin
538 (Amk), and Streptomycin (Str) was also assayed. We observed 50% (1/2), 60% (5/5), 100% (1/1),
539 87.5% (7/8) of the isolates exhibiting complete or intermediate resistance to Gen, Kan, Amk, and
540 Str, respectively, were isolated from urobiomes for which WGMS resistome profiling detected
541 ARGs conferring resistance (Figure 7C). We observed that 27.3% (3/11) and 33.3% (2/6) of the
542 isolates with complete or intermediate resistance to the fluoroquinolones, Ciprofloxacin and
543 Levofloxacin, were isolated from urobiomes for which WGMS resistome profiling detected ARGs

544 conferring resistance (Figure 7C). However, because GROOT does not detect single nucleotide
545 polymorphisms (SNPs) and fluoroquinolone resistance is often conferred by SNPs in the
546 quinolone resistance-determining regions (QRDR) of the genes encoding gyrase and
547 topoisomerase I, fluoroquinolone ARG identification was less sensitive (Correia et al., 2017).
548 Relatively few urobiomes harbored resistance factors to macrolides, which are not clinically used
549 in the treatment of Gram-negative infections (Arsic et al., 2018). However, while 60% (3/5) of the
550 urobiomes dominated by Gram-positive uropathogens harbored macrolide ARGs, such as *mphA*
551 and *erm* genes, we observed that all Gram-positive isolates were resistant to erythromycin.
552 Tetracycline and phenicol ARGs were less common in the WGMS data and we observed little
553 resistance to these antibiotics among tested isolates (Figure 7C). Taken together, these data
554 suggest an overall fair accuracy of prediction of antibiotic resistance phenotype by WGMS ARG
555 analysis that varies depending on drug class.

556

557 **Discussion**

558 This study provides a robust survey of the urobiome in health and rUTI using a cross-sectional,
559 controlled human cohort of postmenopausal women. This age group is particularly burdened by
560 UTI and rUTI with more than 50% of UTIs progressing into rUTI (Gaitonde et al., 2019). Given
561 that many postmenopausal women experience UTIs, the frequency of progression into rUTI
562 imparts a significant impact on quality of life and if treatment is unsuccessful can lead to life
563 threatening urosepsis. However, few postmenopausal women experiencing rUTI find rapid relief
564 from the cycles of infection and millions of patients suffer the significant medical burden of a
565 chronic disease. A decade of research has identified and characterized the urobiome; the
566 microbial communities inhabiting the urinary tract (Brubaker and Wolfe, 2017; Hilt et al., 2014;
567 Lewis et al., 2013; Price et al., 2019; Siddiqui et al., 2011; Wolfe et al., 2012). Through these
568 research endeavors, it has become evident that the urobiome is involved or affected by urinary
569 tract disease. Given the interconnection between host health and microbiome composition, the
570 urobiome has drawn significant attention in further understanding the pathobiology of UTI and
571 rUTI (Thomas-White et al., 2018). Currently, most metagenomic studies of the female urobiome
572 are performed in mostly younger or mixed age cohorts with little focused representation of
573 postmenopausal women (Vaughan et al., 2021). This lack of focus on postmenopausal women
574 leaves critical gaps in our knowledge of a demographic that is heavily impacted by UTI, rUTI, and
575 other urological diseases. In a focused effort to understand the postmenopausal urobiome
576 ecology and function in rUTI, we used a comprehensive approach, coupling whole genome
577 metagenomic sequencing (WGMS) with advanced urine culture, mass spectrometry-based

578 metabolite profiling, and a combination of traditional and Bayesian statistical methodologies to
579 provide an unbiased, robust survey of the postmenopausal urobiome during rUTI pathology. We
580 generated a unique, controlled human cohort which models both the active infection (rUTI
581 Relapse) and intervening stages of rUTI (rUTI Remission) in postmenopausal women, a
582 demographic which is underrepresented in infection biology, microbiome, and clinical research.

583 While the urobiome has been importantly and robustly characterized using bacterial 16S
584 amplicon sequencing, few WGMS studies have been reported (Ammitzboll et al., 2021; Moustafa
585 et al., 2018; Siddiqui et al., 2011; Thomas-White et al., 2020; Vaughan et al., 2021). This unbiased
586 approach allows for the profiling of prokaryotic, eukaryotic, archaeal, and viral taxa present in the
587 sample. Beyond taxonomic profiling, WGMS also allows the characterization of the functional,
588 genetic content of the urobiome (Neugent et al., 2020; Quince et al., 2017). By looking beyond
589 the species-level taxonomic composition, we can define metabolic pathways, virulence factors,
590 and genes critical in urobiome health and urinary tract pathology using WGMS.

591 Taxonomic profiling by WGMS is a very sensitive technique to profile the ecology of a microbial
592 niche. However, *in silico* analysis of metagenomic sequencing data can suffer from database bias
593 and does not have the ability to distinguish living from dead microbial community members
594 (Quince et al., 2017). To address these issues, we combined a bioinformatics analysis of deeply
595 sequenced WGMS dataset with advanced urine culture based on a modified version of the
596 previously reported EQUC protocols (Hilt et al., 2014). This hybrid approach was able to confirm
597 the presence of 93.9% of the genera observed at >5% relative abundance in the aggregate
598 metagenomic data. Our culturing efforts also led to the generation of an extensive biobank of 904
599 speciated and cryopreserved pure isolates, a unique resource for the field.

600 Our taxonomic analysis of the three groups determined that bacteria make up the majority of
601 the non-human, non-viral metagenome of the postmenopausal urobiome. The detected bacterial
602 taxa across the three cohort groups were mainly members of the Phyla *Firmicutes*, *Actinobacteria*,
603 and *Proteobacteria*. The main uropathogen detected in the rUTI Relapse group was UPEC, an
604 observation consistent with the fact that UPEC is responsible for 75% of all UTIs (Flores-Mireles
605 et al., 2015). The urobiomes of the No UTI History and rUTI Remission groups were either
606 dominated by a single bacterial species or were relatively diverse. Both the No UTI History and
607 rUTI Remission group exhibited similar subsets of patients dominated by species of vaginal
608 *Lactobacillus*, *Gardnerella*, and *Bifidobacterium*, which mainly consisted of the species *L.*
609 *crispatus*, *L. gasseri*, *L. iners*, *B. breve*, *B. dentium*, *B. longum*, and *G. vaginalis* (Ravel et al.,
610 2011). These data support the observations by Thomas-White et al. of an interconnected
611 urogenital microbiome (Thomas-White et al., 2018). Many of the diverse urobiomes exhibited the

612 presence of streptococci, such as, *S. agalactiae* and *S. anginosus*. These species of streptococci
613 are not only known uropathogens but have also been linked to vaginal dysbiosis (Gilbert et al.,
614 2021). We detected relatively small abundances of fungal and archaeal taxa. Currently, little is
615 known about the impact or function of fungal and archaeal taxa in the urobiome, particularly of
616 postmenopausal women. This represents an area of significant interest for future research.

617 Ecological modeling with alpha- and beta-diversity metrics found that the urobiomes of the rUTI
618 Relapse group exhibited a less diverse and taxonomically distinct signature than those of the No
619 UTI History and rUTI Remission groups. This can be attributed to uropathogen domination of the
620 urobiome during infection. A critical question for future research will be to determine the
621 longitudinal impact of infection on the underlying urobiome. Interestingly, the No UTI History and
622 rUTI Remission groups were virtually indistinguishable in alpha- and beta-diversity measures.
623 This observation indicates that the large-scale taxonomic structure of the urobiome is relatively
624 similar between women with and without rUTI history. This analysis does not measure fine-scale
625 taxonomic changes as information is lost during the dimensionality reduction techniques used for
626 beta-diversity assessment. Further, this analysis does not consider possible changes in the
627 functional potential of the urobiome, such as metabolic enrichment or antimicrobial resistance.

628 Within microbial communities, co-occurrence is often observed between different taxa that
629 presumably mutually benefit one another. The opposite, e.g., mutual exclusivity is also observed
630 among microbial communities and is attributed to inter-taxa competition during the colonization
631 of a given niche (Faust et al., 2012). Little is currently known of taxonomic associations within the
632 urobiome of postmenopausal women. Interestingly, we observed three non-interacting bacterial
633 co-occurrence networks in the urobiomes of the No UTI history and rUTI Remission cohort
634 groups. These networks include a cluster of genera known to be members of the human gut
635 microbiome: *Bacteroides*, *Collinsella*, *Lachnospiraceae*, *Eggerthella*, *Eubacterium*, *Blautia*, and
636 *Subdoligranulum*. The largest co-occurring bacterial cluster consisted mainly of known members
637 of the female urogenital microbiome. Interestingly, these taxa clustered strongly around the
638 genus, *Peptoniphilus*, a member of the vaginal microbiome believed to be associated with
639 bacterial vaginosis (Marrazzo et al., 2008; Onderdonk et al., 2016). The third cluster detected was
640 a pairwise association between the genera *Gardnerella* and *Atopobium*, two taxa again known to
641 be associated with bacterial vaginosis (Bradshaw et al., 2006). Of note, we did not detect any co-
642 occurrence networks that included *Lactobacillus*. We hypothesize that this is due to the tendency
643 for lactobacilli to dominate the microbial community and will require further research to
644 mechanistically understand. A body of work has characterized the ability of vaginal lactobacilli to
645 protect against bacterial vaginosis by the secretion of D-lactate among other mechanisms (Atassi

646 et al., 2019; Daniel S. C. Butler, 2016; Edwards et al., 2019; Jespers et al., 2015). In the vaginal
647 environment, the major *Lactobacillus* spp., *L. crispatus*, *L. iners*, *L. gasseri*, and *L. jensenii*, are
648 critical for maintaining vaginal pH and resisting invasive pathogens associated with bacterial
649 vaginosis (Ravel et al., 2011). It is still largely unknown if these same *Lactobacillus* species play
650 a similar protective role in the urobiome.

651 We hypothesized that rUTI would leave a detectable taxonomic imprint of the underlying
652 urobiome. Our initial alpha- and beta- diversity analysis did not detect any significant differences
653 between the No UTI History and rUTI Remission groups. However, this analysis is not sensitive
654 to individual taxa-level enrichments. Differential taxonomic enrichment detected genus- and
655 species-level taxonomic biomarkers enriched in women with rUTI history. We observed genus-
656 level enrichments for many of the known uropathogenic species in the rUTI Remission group as
657 compared to the No UTI History group. These enriched uropathogenic genera included *Klebsiella*,
658 *Escherichia*, and *Enterococcus*. It is unclear whether these uropathogen enrichments are
659 representative of persisting populations of previous infections. The enrichment of the genus
660 *Lactobacillus* in the No UTI History group was also expected given the role many vaginal
661 lactobacilli play in protection from bacterial vaginosis (Jespers et al., 2015). At the species-level,
662 we observed that *L. vaginalis* and *L. crispatus*, two species associated with vaginal health, were
663 strongly enriched among the women of the No UTI History group (Jespers et al., 2015).
664 Conversely, in the rUTI Remission group we observed strong species-level enrichments of
665 *Ureaplasma parvum*, *Anaerococcus hydrogenalis*, *E. faecalis*, *S. hominis*, *Peptoniphilus*
666 *lacrimalis*, and *Anaerococcus prevotii*, suggesting that a history of rUTI changes the underlying
667 taxonomic structure of the urobiome. Interestingly a 2021 report by Vaughan et al. studying the
668 urobiome of postmenopausal women with rUTI identified multiple taxonomic differences
669 associated with rUTI compared to controls, including differences in the order, *Bacteroidales*, and
670 the family, *Prevotellaceae* (Vaughan et al., 2021).

671 Postmenopausal women are disproportionately affected by rUTI (Glover et al., 2014). Evidence
672 suggests that approximately 50% of UTIs experienced by postmenopausal women will progress
673 into rUTI (Glover et al., 2014; Ikaheimo et al., 1996). These associative observations beg
674 questions about menopausal changes which may make PM women more susceptible to rUTI.
675 One major physiological change during menopause is a dramatic decrease in circulating levels of
676 the sex hormones in the estrogen family. Menopause-associated decreases in estrogen levels
677 are associated with many changes in physiology, including vasomotor symptoms, sleeping
678 disorders, sexual health, urogenital discomfort, and quality of life (Fait, 2019). Estrogen hormone
679 therapy (EHT) is a common medical intervention many PM women use to treat discomfort

680 associated with menopause (Fait, 2019). Our analysis of cohort-associated metadata found a
681 strong link between EHT use and the presence of *Lactobacillus* in the urobiome of non-infected
682 patients. These observations support those made by Thomas-White et al. and are of particular
683 interest to research endeavors seeking to identify possible UTI-protective members of the urinary
684 and urogenital tract microbial communities (Thomas-White et al., 2020). Lactobacilli control the
685 local chemical environment of the vagina and are responsible for not only maintaining an acidic
686 pH, but also secrete large amounts of the antimicrobial D (-) lactate isomer (Amabebe and
687 Anumba, 2018). A 2019 report by Edwards et. al showed that vaginal *L.crispatus* directly confers
688 protection against *Chlamydia trachomatis* infection through the secretion of large amounts of D (-
689) lactate (Edwards et al., 2019). Given the prevalence of vaginal species of lactobacilli (*i.e.* *L.*
690 *crispatus*, *L. gasseri*) in the urobiome, it is possible that these species play a similar role in
691 preventing uropathogen colonization the urinary tract, and that disruptions in urogenital lactobacilli
692 populations may increase susceptibility to UTI and rUTI (Thomas-White et al., 2018). In the
693 present study, we found that the two largest sources of variances in taxonomic ecology between
694 groups were the genera *Escherichia* and *Lactobacillus*. The variance explained by *Escherichia*
695 abundance can be attributed to UPEC infection whereas we the presence of *Lactobacillus spp.*
696 was strongly predicted by EHT use. We further identify *L. crispatus* and *L. vaginalis* as uniquely
697 associated with EHT use. Interestingly, EHT(-) women exhibited urobiome enrichment of
698 streptococci, such as *S. infantis* and *S. mitis/oralis/pneumoniae*. We also observed that EHT(-)
699 women were enriched for *A. vaginae*, a Gram-positive species associated with *G. vaginalis* in
700 bacterial vaginosis. These differential taxonomic enrichment signatures may suggest a level of
701 urobiome dysbiosis among the postmenopausal women not using EHT. Future work is needed to
702 understand the taxonomic perturbations of the urobiome in rUTI pathology.

703 The cohort studied here exhibited women using three different modalities of EHT (oral,
704 transdermal patch, and vaginal cream). Our findings suggest that oral and patch EHT modalities
705 are associated with significant enrichment of *Lactobacillus* in the urobiome. However, we
706 observed a large amount of variance in the abundance of *Lactobacillus* among patients taking the
707 vaginal modality of EHT. We hypothesized that EHT modalities may differ in dosage, composition,
708 patient compliance, or primary metabolism. Oral and patch EHT modalities used by women in the
709 cohort contained 17 β -estradiol as the active ingredient. However, vaginal EHT modalities include
710 two estrogen compositions. 64.7% of vaginal EHT(+) women used a 17 β -estradiol cream while
711 35.3% of vaginal EHT(+) women used conjugated estrogens creams, which contain mainly equilin
712 sulfate and estrone sulfate as the active ingredients (Whittaker et al., 1980). Circulating estrogens
713 are metabolized in the liver and conjugated with polar chemical groups, such as sulfates or

714 glucuronides, for urinary excretion (Raftogianis et al., 2000). Our data suggests that both oral and
715 patch EHT modalities are associated with elevated excreted urinary estrogen conjugates, while
716 vaginal EHT modalities were not. In a 2021 report, Anglim et al. found no difference in urinary
717 lactobacilli among postmenopausal women with and without rUTI taking vaginal EHT compared
718 to baseline controls (Anglim et al., 2021). However, Thomas-White et al. reported a significant
719 enrichment of lactobacilli in the bladders of postmenopausal women with overactive bladder
720 symptoms using vaginal EHT (Thomas-White et al., 2020). These results along with our report
721 suggest nuances in the association between urinary lactobacilli and EHT that merit future
722 mechanistic research.

723 We further performed an exploratory correlation analysis to globally determine the taxa
724 associated with excreted urinary estrogen conjugates. Interestingly, we found that disease state
725 affected the results of this analysis with the No UTI History and rUTI Remission groups exhibiting
726 different patterns of taxonomic association with excreted urinary estrogen. The species *B. breve*,
727 *L. iners*, *L. crispatus*, and *L. gasseri*, correlated with urinary estrogen conjugates in the No UTI
728 history group only. We did not observe strong taxonomic associations with urinary estrogens in
729 the rUTI Remission group. We hypothesize that this may be due to the fact the rUTI Remission
730 EHT(+) women were predominantly taking vaginal EHT, which we observe to not be strongly
731 associated with urinary lactobacilli. This observation may also be attributable to perturbations of
732 the underlying urobiome by the history of infection and treatment in the rUTI Remission patients.

733 The use of WGMS allowed for the assessment of the total genetic potential of the urobiome
734 between disease states (Quince et al., 2017). Our analysis found that cohort urobiomes cluster
735 similarly by function as they do by taxonomy. Of note, the metabolic pathways facilitating this
736 distinct clustering of the rUTI relapse group away from the No UTI history and rUTI Remission
737 groups were mainly LPS biosynthesis, the TCA cycle, sugar utilization, and biosynthesis of
738 electron carriers, such as demethylmenaquinol-8. This pattern of discrimination may represent a
739 metabolic signature of carbon sources and central metabolism shared among uropathogen-
740 dominated microbial communities. Pairwise differential enrichment analysis revealed that
741 compared to the urobiomes of the No UTI history group, the urobiomes of the rUTI Remission
742 group exhibited greater metabolic potential for the degradation of carbohydrates, biosynthesis of
743 electron carriers, production of cell envelope, and polysaccharide metabolism among others.
744 These data suggest that a history of rUTI, even in the absence of an active infection, alters
745 urobiome functional potential. Future work may focus on understanding whether these alterations
746 are signatures of dysbiosis or sensitization factors for future rUTI Relapse events. Interestingly,
747 we observed that L-lysine biosynthesis II (acetylase variant pathway observed among *Firmicutes*

748 (Bartlett and White, 1985) was very strongly enriched in the No UTI History urobiomes, a
749 discriminatory feature that was also found in comparison to the active infections of the rUTI
750 Relapse urobiomes. Finally, the No UTI History urobiomes exhibited strong enrichments for
751 nucleotide biosynthesis pathways while the rUTI Relapse cohort were enriched for nucleotide
752 degradation pathways. These data may suggest critical differences in the metabolic phenotypes
753 of commensal and uropathogenic members of the urobiome.

754 A critical functional analysis enabled by WGMS is resistome profiling. This is essential for rUTI,
755 which is most often managed by antibiotic therapy (Waller et al., 2018). The cyclic nature of rUTI
756 treated by frequent antibiotic regimens is thought to facilitate the evolution of antibiotic resistance
757 within the urobiome and among uropathogens. Consequences of acquired antibiotic resistance
758 include treatment failure, a need for urgent escalation of therapeutic strategies, and if
759 unsuccessful, cystectomy or life-threatening urosepsis. Currently, there is no single dataset
760 profiling the rUTI-associated antimicrobial resistance genes (ARGs) encoded in the urobiomes of
761 a controlled cohort of postmenopausal women. As expected, we found that the resistome of the
762 infected urobiomes of the rUTI Relapse contained significantly more ARGs than the No UTI
763 History group. Interestingly, we also found that the rUTI Remission urobiome also harbored a
764 significantly larger resistome than the No UTI History urobiomes. This suggests that even in the
765 absence of infection, a history of rUTI is associated with significantly more urobiome ARGs than
766 found in healthy comparators with no lifetime history of UTI. rUTI Relapse urobiomes exhibited
767 significant enrichments for the TEM β -lactamase alleles. It should be noted that the analytical
768 pipeline used was not able to distinguish between TEM alleles. Interestingly, rUTI Relapse
769 urobiomes also exhibited significant enrichments for ARGs which confer resistance to
770 sulfonamide antibiotics, such as the frontline antibiotic, sulfamethoxazole. Phenotypic analysis
771 showed that bacterial isolates generated from the rUTI Relapse cohort exhibited similar antibiotic
772 resistance phenotypes as what WGMS predicted. These data suggest that, at least among
773 uropathogenic bacteria, antibiotic resistance predicted by WGMS resistome profiling was
774 reasonably consistent with observed phenotypes. One major limitation of currently available
775 resistome profiling pipelines for metagenomic datasets; however, is that they are limited to
776 detecting ARGs and do not detect antibiotic resistances conferred by point mutations. This
777 limitation makes detection of quinolone resistance by this method incomplete. Further study is
778 needed to understand the evolution of the resistome associated with rUTI

779 This work aimed to survey the taxonomic and functional ecology of the urobiome associated
780 with rUTI and rUTI history through WGMS analysis of a clinically relevant group of
781 postmenopausal women. These robust sequencing and analytical datasets, associated clinical

782 metadata, and extensive microbial isolate collection represent an important resource for the field.
783 Our analysis has identified taxonomic and functional biomarkers associated with rUTI history, as
784 well as a set of putatively protective taxa correlated with particular modalities of EHT. We also
785 find that a history of rUTI significantly alters the number of and composition of resistance genes
786 encoded in the urobiome, an observation with implications towards future and current treatment
787 paradigms rUTI. Taken together, this work provides robust foundation for further mechanistic
788 studies of how the urobiome is associated with rUTI pathobiology and perhaps may serve as a
789 resource for the development of urobiome-aware alternative therapies for a disease that affects
790 millions of women worldwide.

791

792 **Methods**

793 **Patient Recruitment and Cohort Curation**

794 The current study is approved under IRBs STU032016-006 (University of Texas Southwestern
795 Medical Center) and 19MR0011 (University of Texas at Dallas). To estimate the number of
796 patients needed to enroll into each cohort group and predict statistical power, we performed a
797 series of power analyses using the 'pwr' package (<https://github.com/heliosdrm/pwr>) in the R-
798 statistical language based on ranging effect sizes from small to large for both multivariate analysis
799 of 3 groups with equal sample size and pairwise-based comparisons of two groups. Balancing
800 cost and clinical feasibility with predicted statistical power, we chose a sample size of 25 for each
801 cohort group. Patients were recruited from the Urology Clinic at University of Texas Southwestern
802 Medical Center between April 2018 and October 2019. Written informed consent was obtained
803 from each patient prior to recruitment into the study cohorts. All patients were postmenopausal
804 females. The following set of exclusion criteria were used to initially screen patient's candidacy
805 for enrollment into the cohort: pre- or perimenopausal status; antibiotic exposure within the 4
806 weeks prior to urine sample donation unless an active infection was detected by culture; pelvic
807 malignancy or history of pelvic radiation within 3 years before urine sample donation; most recent
808 post void residual (PVR) greater than 100 mL; greater than stage 2 prolapse; pelvic procedure for
809 incontinence within 6 months prior to urine sample donation; use of intermittent catheterization;
810 neurogenic bladder; any upper urinary tract abnormality which may explain rUTI; and Diabetes
811 Mellitus (DM) type 1 or 2. All urine samples were obtained by clean-catch midstream urine
812 collection and therefore were representative of the urogenital microbiome, rather than specifically
813 just the bladder microbiome. Patients were educated about the cleaning and urine collection
814 needs for this sampling technique prior to urine collection. Urine samples were stored at 4°C for
815 no more than 4 hours before sample processing, aliquoting, and biobanking at -80°C.

816 Patients were further vetted by self-reporting of UTI history, mining clinical history from
817 electronic patient records, clinical (standard) urine culture, and urine culture on Chromogenic agar
818 (BBL CHROMagar Orientation, BD). Clinical urine culture was performed on samples from all
819 patients with active UTI symptoms by the Clinical Microbiology Laboratory at UT Southwestern
820 Medical Center. Group assignment criteria were as follows. No UTI History: no self-reported or
821 clinical history of UTI, no UTI symptoms at the time of urine collection. rUTI Remission: recent
822 history of rUTI, no UTI symptoms at time of sample collection. rUTI Relapse: recent history of
823 rUTI, active UTI symptoms at time of urine collection, positive clinical urine culture. Positive urine
824 culture was defined as $>10^4$ bacterial CFU/mL.

825

826 **Advanced Urine Culture, Isolate Identification, and Isolate Biobanking**

827 Glycerol-stocked urine samples (stored at -80°C) were thawed at room temperature, and then
828 diluted 1:3 and 1:30 in sterile 1X Phosphate Buffered Saline to adjust plating density for high and
829 low biomass samples. 100 μl of urine from each dilution was plated onto blood agar plates (BAP),
830 CHROMagar Orientation, De Man, Rogosa, and Sharpe (MRS) agar, Rabbit BAP (R-BAP), BD
831 BBL CDC anaerobe blood agar (CDC AN-BAP), and Columbia Colistin Naladixic Acid Agar
832 (CNA). Following plating, BAP was incubated in ambient and 5% CO_2 atmospheres, CHROMagar
833 Orientation in 5% CO_2 , MRS and R-BAP in microaerophilic conditions, BD BBL CDC anaerobe
834 blood agar (CDC AN-BAP) in microaerophilic and anaerobic conditions and CNA in all four
835 atmospheric conditions. Plates were incubated at 35°C for 4 days in the respective atmosphere.
836 It should be noted that we were unable to culture *Gardnerella spp.* using these methods. However,
837 WGMS profiling frequently detected *G. vaginalis* in the sampled urobiomes. For targeted isolation
838 of *Gardnerella spp.*, 100 μl urine was plated onto Human polysorbate-80 (HBT) bilayer medium in
839 microaerophilic atmosphere for 3 days. To isolate fungal species, 100 μl urine was plated onto
840 Brain Heart Infusion Agar supplemented with 20 g/L glucose and 50 mg/ μl of chloramphenicol
841 (BHIg-Cam) and incubated at 5% CO_2 for 3 days.

842 Bacterial identification was performed by PCR amplification and Sanger sequencing of the 16S
843 rRNA gene from well-isolated colonies as described previously (De Nisco et al., 2019). Briefly,
844 16S rRNA gene was amplified using primers 8F (5'-AGAGTTTGATCCTGGCTCAG-3') and
845 1492R (5'-GGTTACCTTGTTACGACTT-3') by colony PCR (Vaishnav et al., 2011) using
846 DreamTaq Master Mix (ThermoFisher Scientific) and 0.2 μM primers. Amplicon size was
847 confirmed on 1% agarose gel, followed by gel purification (Bio basic) and Sanger Sequencing
848 (Genewiz) using the 8F primer. Sequences were analyzed using BLASTn against the NCBI 16S
849 ribosomal RNA (Bacteria and Archaea) database.

850 For fungal identification, ITS1 and ITS2 regions were amplified using the primer sequences
851 ITS1: 5'-TCCGTAGGTGAACCTGCGG-3' and ITS2: 5'-GCTGCGTTCTTCATCGATGC-3' from
852 well-isolated colonies and Sanger sequenced (Genewiz). Sequences were analyzed using
853 BLASTn against the NCBI ITS from Fungi type and reference material database.

854 All the isolated and taxonomically identified isolates (n=904) were assigned a distinct ID and
855 biobanked at -80°C in glycerol. The isolates were grown in Brain Heart Infusion broth, Tryptic Soy
856 Broth (BD 211825), MRS broth or NYCIII according to their growth preferences and stocked in
857 16% sterile glycerol for long-term storage at -80C.

858

859 **Metagenomic DNA Isolation, Library Construction, and Sequencing**

860 Prior to WGMS, we assessed the quality and reproducibility of 3 metagenomic DNA extraction
861 techniques: a modified genomic DNA (gDNA) isolation based on the Qiagen blood and tissue
862 DNAeasy Kit, the Zymo Research DNA/RNA microbiome miniprep, and a modified
863 phenol/chloroform/isoamyl alcohol extraction as demonstrated by Moustafa et al. (Moustafa et al.,
864 2018) After assessing the quality and yield of metagenomic DNA isolated using the three
865 methods, we chose the Zymo Research method. Urine samples were allowed to thaw on ice at
866 4°C overnight. 10-20 mL of urine was centrifuged for 15 minutes at 4000 x g at 4°C. Urine pellets
867 were resuspended in 750 µL of DNA/RNA Shield (Zymo Research), transferred to a bead beating
868 tube, and subjected to ten 30 sec cycles of mechanical bead beating, with 5 min cooling between
869 each cycle. After mechanical lysis, the maximum volume of sample was collected and transferred
870 to a new microcentrifuge tube with DNA/RNA lysis buffer (Zymo). Nucleic acids were purified via
871 the Zymo Research DNA/RNA microbiome miniprep kit per the manufacturer's instruction. Elution
872 of DNA from the column was performed in nuclease-free water and each column was eluted twice
873 to maximize DNA recovery. As a control to internally assess gDNA extraction efficiency and
874 WGMS limit of detection (LOD), gDNA was concurrently extracted from commercially available
875 community standards (ZymoBiomics) using the same methods. gDNA was also extracted from
876 nuclease-free water to account for kit and environmental contamination. All DNA samples were
877 subjected to 16S rRNA gene amplification by PCR and visualized by agarose gel electrophoresis
878 to ensure microbial DNA was present before proceeding with WGMS. DNA yield and purity for all
879 samples were assessed by agarose gel electrophoresis, and by fluorescence-based Qubit
880 quantitation of DNA, RNA, and protein. Prior to library preparation the DNA concentration of each
881 sample was normalized and 20pg of spike-in gDNA was added (Zymo Research High Bacterial
882 Load Spike-in), which contains gDNA from the bacterial species *Imchella halotolerans* and
883 *Allobacillus halotolerans*, which are known to not be associated with humans.

884 WGMS was performed at the University of Texas at Dallas Genome Center using 2x150 bp
885 paired-end reads on a Illumina NextSeq 500. Library preparation was performed using Nextera
886 DNA Flex kit. Library preparation of the entire cohort and community standard and water controls
887 was distributed over 2 batches with overlapping samples. All samples were sequenced using
888 2x150 base pair paired-end sequencing in high output mode with a target of ≥ 50 million paired
889 end reads per sample.

890

891 **Bioinformatic Analyses**

892 All taxonomic, functional, and resistome bioinformatic analyses were performed on an in-house
893 Dell PowerEdge T630 server tower with 256GB RAM, 12 core Intel Xenon processor with 16TB
894 storage capacity or at the Texas Advanced Computing Center (TACC).

895 **Data Preprocessing**

896 The fastq files were checked for read quality, adapter content, GC contents, species
897 contamination using fastqc (v0.11.2) and fastq_screen (v0.4.4) (Andrews, 2015; Wingett and
898 Andrews, 2018). Low-quality reads (a quality score of less than Q20) and adapter were removed
899 using Trim galore (v 0.4.4) (Krueger). Human DNA sequences were removed using KneadData
900 (Huttenhower).

901 **Taxonomic Profiling, Ecological Modeling, and Co-Occurrence Analysis**

902 The taxonomic assignment and estimation of composition of microbial species present in each
903 sample was performed using MetaPhlan2 (Segata et al., 2012). MetaPhlan2 estimates the
904 relative abundance of species by mapping the metagenomic reads against a clade specific marker
905 gene database. The database consists of bacterial, archaeal, viral and eukaryotic genomes. We
906 further used merge_metaphlan_tables module of MetaPhlan2 to combine the relative abundance
907 estimates of samples in a cohort into one table.

908 To identify kit, environmental, and background contaminating taxonomic signals, we sequenced
909 a water sample which was randomly inserted into the metagenomic DNA preparation protocol.
910 Sequencing and taxonomic analysis of this sample revealed known kit and environmental
911 contaminants, such as *Delftia*, *Stenotrophomonas*, *Ralstonia*, *Bradyrhizobium*, and others (Salter
912 et al., 2014). Unless a known member of the human microbiome, these taxa were censored from
913 the entire dataset. We further assessed the WGMS limit of reliable detection using a commercially
914 available log community standard (ZymoBiomics), which is composed of multiple Gram-positive
915 and Gram-negative bacterial and fungi. We observed a strong linear correlation between the
916 theoretical and observed relative abundance above 0.001%. We therefore set a relative
917 abundance threshold of 0.001% for a taxon to be considered as detected within a sample.

918 Species-level MetaPhlAn 2 taxonomic assignments were not included in analysis if they were
919 “unclassified”.

920 Alpha-diversity analysis was performed at the species-level using phyloseq (version 1.16.2)
921 (McMurdie and Holmes, 2013). Beta-diversity analysis was performed using DPCoA on the
922 species-level taxonomic relative abundance dataset using phyloseq (version 1.16.2)(McMurdie
923 and Holmes, 2013). Taxonomic co-occurrence was performed with CCREPE pipeline using the
924 Pearson correlation and compositionally corrected P-values
925 (<https://github.com/biobakery/biobakery/wiki/ccrepe#22-ccrepe-function>). Network analysis of
926 taxonomic co-occurrences was performed using CytoScape (Version 3.8.2) with edges defined
927 by the correlation coefficients between taxa nodes.

928 **Functional Metabolic Profiling**

929 Functional metabolic profiling was performed using HUMAnN 2.0 (Franzosa et al., 2018).
930 HUMAnN2 uses a tiered approach to identify the functional profile of microbial communities.
931 Firstly, it maps the sample reads to clade specific markers and creates a database of pangenomes
932 for each sample. In the second tier, it performs the nucleotide level mapping of samples reads
933 against pangenome database. Lastly, a translated search against Uniref90 is performed for
934 unaligned reads in each sample (Suzek et al., 2015). The output result is the mapping of reads to
935 gene sequences with known taxonomy. The reads are normalized to gene sequence length to
936 give an estimate of per-organism and community total gene family abundance. Next, gene
937 families are analyzed to reconstruct and quantify metabolic pathways using MetaCyc (Caspi et
938 al., 2018). Different modules of HUMAnN such as `humann2_join_table` and
939 `humann2_renorm_table` were used to merge the pathway abundance of all the samples in a
940 cohort and normalize the abundance to cpm respectively. We filtered the results to only include
941 pathways whose taxonomic range included bacteria. We further censored pathways which were
942 specifically associated with a particular taxon due to database bias toward commonly isolated
943 and studied species. PCA of functional pathways was performed on the pathway level relative
944 abundance dataset using `factroextra` ([https://cran.r-](https://cran.r-project.org/web/packages/factoextra/readme/README.html)
945 [project.org/web/packages/factoextra/readme/README.html](https://cran.r-project.org/web/packages/factoextra/readme/README.html)). Pathway differential abundance
946 analysis was performed using LEfSe (Segata et al., 2011) on the pathway-level relative
947 abundance dataset. LEfSe uses Kruskal Wallis and Wilcoxon tests to find the differential
948 pathways between microbial communities. Finally, it uses LDA model to rank the pathways.

949 **Resistome Profiling and ARG Enrichment**

950 We used the GROOT (Graphing Resistance Out Of meTagenomes) to generate a profile of
951 antimicrobial resistance genes within the urobiomes of the present study (Rowe and Winn, 2018).

952 The default database ARG-ANNOT was used for alignment of the metagenomics reads.
953 Subsequently GROOT report command was used to generate a profile of antibiotic resistance
954 genes at a read coverage of 90%. Filtering of the GROOT results was performed to insure high
955 confidence in ARG presence within the urobiomes. We used a conservative cutoff of a sufficient
956 amount of reads to generate 10x coverage of an ARG to qualify its detection within a urobiome.
957 We further collapsed alleles of the β -lactamase genes TEM, CTX, OXA, OXY2, SHV, and *cfxA* as
958 well as the aminoglycoside ARG Aac3-IIa and Aac3-IIe alleles into single gene-level features to
959 account for multiple-mapping reads.

960 Bayesian modeling of the resistome data was performed as follows. Resistome data for the
961 three cohorts (Never = 1, Remission = 2, Relapse = 3) consisted of 186 antimicrobial resistance
962 genes (ARG) which were collapsed into family-level genes ($G = 55$). Each cell in the data set
963 contained a binary indicator of no detection (0) or detection (1) of the resistance family-level gene
964 within each patient sample such that $x_{gik} = \{0,1\}$, $g = 1, \dots, 55$, $i = 1, \dots, 25$, $k = 1, 2, 3$ indicates no
965 detection or detection of resistance family-level gene g respectively for sample $i = 1, \dots, 25$ in
966 cohort k .

967 A Bayesian Beta-Bernoulli model with Jeffreys prior was used to model the posterior
968 distributions of group proportions and pairwise differences for the G family-level genes $G =$
969 $1, \dots, 55$. Three posterior inferences were performed. First, we removed any family-level genes
970 that had no significant pairwise contrasts using 95% credible intervals as criteria. We determined
971 that a significant family level-gene does not have zero contained in a 95% credible interval for at
972 least one pairwise contrast. Second, we computed the posterior probability and Bayes Factor (BF)
973 to make inferences on each pairwise contrast of cohort proportions of only the significant family-
974 level genes. The BF computed for each contrast represented the odds of H_1 : “at least one cohort’s
975 proportion for gene g is different” in favor of H_0 : $\omega_{g1} = \omega_{g2} = \omega_{g3}$.

976 **Taxonomic Biomarker Analysis**

977 We applied two methods of taxonomic differential abundance analysis employing the robust and
978 widely used LEfSe pipeline as well as BMDA, a recently described Bayesian model of differential
979 abundance (Li et al., 2019). LEfSe analysis was performed as previously described (Segata et
980 al., 2011). For the BMDA model we first applied the quality control step (detailed in the supplement
981 of Li et al., 2019) to the raw count data. We then fitted the BMDA model, which is a novel Bayesian
982 hierarchical framework that uses a zero-inflated binomial model to model the raw count data and
983 a Gaussian mixture model with feature selection to identify differentially abundant taxa. The
984 BMDA can fully account for zero-inflation, over-dispersion, and varying sequencing depth. We
985 chose weakly informative priors on all parameters of the model to avoid biased results. For model

986 fitting and posterior inference, BMDA implements the Metropolis-Hastings algorithm within a
987 Gibbs sampler. The marginal posterior probability of inclusion (PPI) was used to identify the set
988 of discriminating taxa between the control and disease groups. Marginal PPI is the proportion of
989 MCMC samples in which a taxon is selected to be discriminatory if it is greater than a pre-specified
990 value. We chose a threshold such that the expected Bayesian false discovery rate (FDR) was
991 less than 0.05.

992

993 **Antibiotic susceptibility testing**

994 Assessment of antibiotic (abx) susceptibility was performed via the Kirby-Bauer disk diffusion
995 susceptibility test (Hudzicki, 2009). Antibiotic disks were prepared by aliquoting 10uL of antibiotic
996 stock (GEN 1mg/ml, AMP 1mg/ml, CIP 0.5mg/ml, LVX 0.5mg/ml, ERM 1.5mg/ml, CHL 3mg/ml,
997 TMP/SMX 1.25/23.75mg/ml, NIT 30mg/ml, DOX 3mg/ml) onto the disk in a sterile petri dish and
998 drying at room temperature in the dark. Vehicle control disks were prepared similarly using the
999 diluents of each antibiotic. Strains were streaked from frozen glycerol stocks onto CHROMagar
1000 or Blood Agar (species dependent) and incubated overnight at 37°C in ambient conditions or 35°C
1001 in 5% CO₂. Single, well-isolated colonies were inoculated into 3 mL Brain-Heart-Infusion broth
1002 and incubated at the respective atmospheric conditions for 16 – 18 hours. After incubation,
1003 cultures were normalized to 0.5 McFarland standard, washed, and resuspended in sterile 1X
1004 Phosphate-Buffered Saline (PBS). 150 µL of standardized culture were pipetted onto 150 mm
1005 Mueller-Hinton Agar plates and spread using sterile glass beads. Plates were dried in sterile
1006 conditions before abx-impregnated disks were placed on the surface of the agar. *E. coli* strain
1007 ATCC25922 was used for quality and vehicle controls. Sterile 1X PBS was plated as sterility
1008 control. Plates were incubated inverted per the recommendations of Clinical and Laboratory
1009 Standards Institute (CLSI) M100-ED30: 2020 Performance Standards for Antimicrobial
1010 Susceptibility Testing, 30th Edition
1011 (<https://clsi.org/standards/products/microbiology/documents/m100/>). After incubation,
1012 antimicrobial susceptibility was evaluated by measurement of the zone of inhibition and using
1013 CLSI established zone diameter breakpoints.

1014

1015 **Liquid Chromatography Mass Spectrometry Measurement of Estrogen Metabolites**

1016 Direct measurement of urinary estrogen metabolites was performed via a modification of
1017 previously reported methods(van der Berg et al., 2020). Briefly, urine (500 µL) was diluted and
1018 spiked with 100 ng stable isotope-labeled internal standards of d3-Estrone 3-Glucuronide and d4-
1019 Estradiol 3-Sulfate. Diluted and spiked samples were loaded onto an equilibrated Phenomenex

1020 C18 cartridge for solid phase extraction to separate conjugated estrogens. Following aqueous
1021 methanolic extraction of estrogen conjugates and non-polar extraction of free estrogens with
1022 methanolic acetone, fractions were dried by vacuum centrifugation and prepared for LC-MS/MS
1023 analysis. Estrogen conjugates (sulfates and glucuronides) were directly assayed using a curated
1024 and optimized MRM library by LC-MS/MS.

1025 High sensitivity quantitative LC-MS/MS was performed on a Waters Xevo TQ tandem
1026 quadrupole MS lined to an ACQUITY UPLC with a Selectra C8 RP column (100x2.1 mm 1.8 μ m,
1027 UCT). MRM libraries of estrogen conjugates have been curated to include both analytical and
1028 confirmatory transitions for each analyte at optimal retention times to maximize separation. Briefly,
1029 data analysis was performed by integrating the peak area of the analytical transition for each
1030 analyte. Peak areas were normalized to molecular class-matched internal spike-in standards and
1031 mapped to a standard curve to accurately estimate analyte concentration. Urine estrogen
1032 metabolite concentrations were then normalized to urinary creatinine, which was measured by
1033 colorimetric assay (Sigma).

1034

1035 **Statistical Analysis**

1036 Statistical analysis was performed using R statistical programming, GraphPad Prism 9, and
1037 Microsoft Excel. For hypothesis testing, non-parametric Mann-Whitney U-test was used for
1038 pairwise comparisons and the Kruskal-Wallis non-parametric ANOVA with multiple comparison
1039 post-hoc was used to for non-paired and unmatched comparisons of 3 or more groups. Multiple
1040 comparison adjustment was performed using false discover rate (FDR) when appropriate. An
1041 alpha of 0.05 was considered significant to control type I error.

1042

1043 **Acknowledgements**

1044 We wish to acknowledge and sincerely thank the patients who participated in this study. This
1045 work was supported by a research grant from The Welch Foundation, a research grant from the
1046 Foundation for Women's Wellness, NIH grant 1R01DK131267-01, and The University of Texas
1047 at Dallas Startup funds to NJD, the Cecil H. and Ida Green Chair in Systems Biology Science to
1048 KLP, The Felicia and John Cain Distinguished Chair in Women's Health to PZ. We would also
1049 like to thank all the members of the De Nisco and Palmer labs for their helpful and creative input
1050 throughout this study. We would further like to acknowledge and thank the Genome Center at the
1051 University of Texas at Dallas for their invaluable work and assistance in generating the
1052 metagenomic dataset used for this study.

1053

1054 **Author Contributions**

1055 Conceptualization, M.L.N., P.E.Z., K.L.P., N.J.D.; data curation, M.L.N., J.F., A.Kup., A.P.A.;
1056 formal analysis, M.L.N, A.Kumar., K.C.L., C.Z., Q.L., C.X., V.S., N.J.D.; funding acquisition, V.S.,
1057 K.L.P, P.E.Z., N.J.D.; investigation, M.L.N., N.V.H., V.H.N., A.N.; methodology, M.L.N., A.Kumar.,
1058 N.V.H., K.C.L., V.H.N., A.N., B.M.S., Q.L., C.X., V.S., P.E.Z., K.L.P., N.J.D.; project
1059 administration, M.L.N., P.E.Z., N.J.D.; resources, P.E.Z., K.L.P., N.J.D.; software, M.L.N.,
1060 A.Kumar., K.C.L., C.Z., Q.L., C.X.; supervision, Q.L., C.X., V.S., P.E.Z., K.L.P., N.J.D;
1061 validation, M.L.N., N.V.H., K.C.L., C.Z.; visualization, M.L.N., V.H.N.; writing-original draft,
1062 M.L.N., A.K., N.V.H., K.C.L., Q.L., C.X., N.J.D.

1063

1064 **Supplemental materials**

1065 Figure S1. Power analysis and metagenomic dataset characteristics.

1066 Figure S2. Power analysis and metagenomic dataset characteristics.

1067 Figure S3. Taxonomic profiles of detected *Archea*, *Eukaryota*, and Vial species.

1068 Figure S4. Ecological modeling indices among the cohort groups.

1069 Figure S5. Urinary estrogen conjugate concentrations and taxonomic associations.

1070

1071 **Figure legends**

1072 **Figure 1. Study design and summary of genera detected by WGMS and advanced urine**
1073 **culture.** (A) Schematic diagram of rUTI pathobiology cycle depicting periods of active,
1074 symptomatic UTI defined by positive urine culture followed by periods of remission defined by
1075 negative clinical urine culture. (B) Schematic diagram of clinical cohort structure and datasets
1076 generated for the study. (C) Taxonomic cladogram of taxa detected in all sequenced
1077 metagenomes ($n=75$) by Metaphlan2. Node size indicates relative abundance and branch length
1078 is arbitrary. The top 20 genera by average relative abundance are displayed. (D) Venn diagram
1079 depicting the coverage of WGMS metagenomes by advanced urine culture. Coverage is
1080 calculated at the genus level considering all bacterial genera exhibiting relative abundance $>5\%$
1081 by WGMS in at least one patient.

1082

1083 **Figure 2. The bacterial taxonomic profile of rUTI in postmenopausal women.** (A) Genus-
1084 level taxonomic profile of the top 15 bacterial genera among cohort groups (No UTI History ($n=25$),
1085 rUTI Remission ($n=25$), rUTI Relapse ($n=25$)). All genera not within the top 15 are combined into
1086 "Other". (B) Species-level taxonomic profile represented within the top 15 bacterial genera among
1087 cohort groups (No UTI History ($n=25$), rUTI Remission ($n=25$), rUTI Relapse ($n=25$)). All species

1088 not represented within the top 15 genera are combined into “Other”. Alpha-diversity comparison
1089 of the observed species counts (C) and Shannon index (D) between cohort groups (1 = No UTI
1090 History ($n=25$), 2 = rUTI Remission ($n=25$), 3 = rUTI Relapse ($n=25$)). Solid lines represent
1091 medians while dotted lines represent the interquartile range. P -value was generated by Kruskal-
1092 Wallis test with uncorrected Dunn’s multiple correction post hoc. (E) Beta-diversity sample
1093 ordination of the WGMS dataset by Double Principal Coordinate Analysis (DPCoA) in the first two
1094 PCoAs. Each dot represents an individual sample color-coded by group (No UTI history in blue,
1095 rUTI remission in purple, and rUTI relapse in salmon). Vectors (grey) are drawn to represent the
1096 major discriminating loadings (*i.e.* species). (F) Volcano plot depicting co-occurrence of genera
1097 within the WGMS dataset by Pearson correlation. P -value generated by permutation. Red dots
1098 represent associations which were considered significant after FDR correction of the P -value.
1099 Blue dots represent associations which exhibited a nominal P -value less than 0.05, but an FDR-
1100 corrected P -value greater than 0.05. (G) Network analysis of all genera co-occurrence
1101 associations with P -value less than 0.05. Nodes represent genera edges are defined by Pearson
1102 correlation. Node size is proportional to the degree of the node.

1103
1104 **Figure 3. Bayesian modeling detects the taxonomic imprint of rUTI history on the urobiome**
1105 **of postmenopausal women.** (A) Schematic representation of the BMDA model. (B) Bayesian
1106 differential abundance model comparing taxonomic enrichment between the No UTI history
1107 ($n=25$) and rUTI Remission ($n=25$) cohort groups. Dots, indicating the \log_{10} (posterior effect size),
1108 are color-coded by their enrichment in a particular cohort group with taxa enriched in No UTI
1109 history in blue and taxa enriched in rUTI remission. Lines indicate the minima and maxima of the
1110 95% credible interval and PPI denotes posterior probability index.

1111
1112 **Figure 4. Estrogen hormone therapy shapes the urobiome of postmenopausal women.**
1113 (A) Genus-level taxonomic profile of the relative abundance of the top 22 bacterial genera among
1114 women reporting no use of estrogen hormone therapy (EHT(-), $n=21$) and women reporting use
1115 of EHT (EHT(+), $n=29$) among the No UTI History and rUTI Remission groups. All genera not
1116 within the top 22 are combined into “Other”. (B) Taxonomic profile of the relative abundance of
1117 species represented within the top 22 bacterial genera among EHT(-) ($n=21$) and EHT(+) ($n=29$)
1118 non-infected women from the No UTI History and rUTI Remission groups. All species not
1119 represented within the top 22 genera are combined into “Other”. (C) Comparison of the relative
1120 abundance of the genus *Lactobacillus* between EHT(-) (grey) and EHT(+) (pink) women in the No
1121 UTI history and rUTI remission groups. Violin plot depicts the smoothed distribution of the data.

1122 Solid lines represent the median. Dotted lines represent the interquartile range. *P*-value generated
1123 by Wilcoxon rank-sum test. Alpha-diversity comparison of the observed species count (D),
1124 Shannon index (E), and Simpson index (F) between EHT(-) (grey) and EHT(+) (pink) women in
1125 the No UTI history and rUTI remission cohorts. Violin plot depicts the smoothed distribution of the
1126 data. Solid lines represent medians while dotted lines represent the interquartile range. *P*-value
1127 generated by Wilcoxon rank-sum. (G) Two significantly differentially enriched taxa detected by
1128 LEfSe biomarker analysis performed between EHT(-) (grey) and EHT(+) (pink) women in the No
1129 UTI history and rUTI remission groups. LDA denotes the \log_{10} (linear discriminant analysis score)
1130 and the *P*-value was generated by Wilcoxon Rank Sum Test. (H) Differentially enriched taxa
1131 between EHT(-) (grey) and EHT(+) (pink) women in the No UTI history and rUTI remission cohorts
1132 detected by the Bayesian differential abundance model. Dots indicate \log_{10} (posterior effect size)
1133 and PPI denotes posterior probability index. *S. m/o/p* denotes *Streptococcus*
1134 *mitus/oralis/pneumoniae*.

1135
1136 **Figure 5. Distinct taxa-urinary estrogen metabolite associations between postmenopausal**
1137 **women with and without rUTI history.** (A) Comparison of the relative abundance of the genus
1138 *Lactobacillus* between EHT(-) (grey, *n*=21) and EHT(+) (pink, *n*=29) women from the No UTI
1139 History and rUTI Remission groups stratified by EHT modality (Oral, Patch, Vaginal). Error bars
1140 are drawn from minimum to maximum of the data distribution. Boxes represent the interquartile
1141 range. Solid lines denote the median. *P*-value generated by Kruskal-Wallis test with uncorrected
1142 Dunn's multiple correction post hoc. Summed creatinine (Cr)-normalized urinary E1 and E2
1143 conjugates (B), E1 conjugates (C) and E2 conjugates (D) measured in the urine of EHT(-) and
1144 EHT(+) women from the No UTI History and rUTI Remission groups stratified by EHT modality
1145 (Oral (*n*=6), Patch (*n*=6), Vaginal (*n*=17)). Error bars are drawn from minimum to maximum of the
1146 data distribution. Boxes represent the interquartile range. Solid lines denote the median. *P*-value
1147 generated by Kruskal-Wallis test with uncorrected Dunn's multiple correction post hoc. Volcano
1148 plots depicting correlation of bacterial species with summed Cr-normalized urinary E1 and E2
1149 conjugates by Spearman correlation in No UTI History (E) and rUTI remission (F) groups. *P*-value
1150 generated by permutation. Red dots represent significant (*p*<0.05) positive associations. Blue
1151 dots represent significant negative associations. (G) Correlation scatter plots of the association
1152 between *B. breve*, *L. iners*, *L. crispatus*, and *A. prevotti*, and summed creatinine-normalized
1153 urinary E1 and E2 conjugates among No UTI History women (*n*=25) (blue) and rUTI Remission
1154 women (*n*=23) (purple). Linear regression trend line (solid line) is shown with 95% confidence
1155 intervals (dashed lines).

1156

1157 **Figure 6. rUTI history and active infection shape the metabolic potential of the urobiome.**

1158 (A, B) Principal component analysis (PCA) of cohort samples by metagenome-encoded pathway-
1159 level metabolic potential. Depiction of sample ordination and clustering in the first two PCAs in
1160 (A) and vectors (grey) defining major discriminatory loadings (*i.e.* metabolic pathways) in (B). Top
1161 40 differentially enriched pathways detected by LEfSe analysis performed between the No UTI
1162 History (blue, $n=25$) and rUTI Remission (purple, $n=25$) cohort groups (C) and the No UTI History
1163 ($n=25$) and rUTI Relapse (red, $n=25$) cohort groups (D). Pathways presented exhibit an FDR-
1164 corrected P -values less than 0.05. LDA score indicates \log_{10} (linear discriminant analysis score).

1165

1166 **Figure 7. rUTI history and active infection shape the resistome of the postmenopausal**

1167 **urobiome.** (A) Comparison of the observed Antibiotic Resistance Genes (ARGs) detected within
1168 the urobiomes of the No UTI History ($n=25$), rUTI Remission ($n=25$), and rUTI Relapse ($n=25$)
1169 cohort groups. Violin plot depicts the smoothed distribution of the data. Solid lines represent
1170 median while dotted lines represent the interquartile range. P -value was generated by Kruskal-
1171 Wallis test with uncorrected Dunn's multiple correction post hoc. (B) Bayesian differential
1172 enrichment analysis of ARG presence within the urobiomes of the No UTI History ($n=25$), rUTI
1173 Remission ($n=25$), and rUTI Relapse ($n=25$) cohort groups. Group comparisons are were
1174 determined by the difference in ARG(+) proportion within a pairwise group comparison. 95%
1175 credible intervals, Bayes factor, and posterior probability are presented for interpretation of
1176 Bayesian analysis. P -value generated by the Fisher Exact test is also provided. (C) Phenotypic
1177 assessment of the agreement between urobiome ARG detection and antibiotic resistance of
1178 isolates of the most abundant uropathogen species present in each patient in the rUTI Relapse
1179 cohort group ($n=23$, *E. coli* ($n=15$), *Klebsiella* ($n=3$), *Streptococcus* ($n=3$), *E. faecalis* ($n=1$), *S.*
1180 *epidermidis* ($n=1$)). Upper diagonal colors represent WGMS GROOT profiling results (blue = ARG
1181 (+), white = ARG(-)). Lower diagonal color represents Isolate Phenotype (red = resistant, yellow
1182 = intermediate resistance, white = sensitive, grey = not tested). Amp, Ampicillin; Cfx, Cefixime;
1183 Cex, Cephalexin; TMP/SMX, Trimethoprim/sulfamethoxazole; Gen, Gentamicin; Kan,
1184 Kanamycin; Amk, Amikacin; Str, Streptomycin; Cip, Ciprofloxacin; Lvx, Levofloxacin; Erm,
1185 Erythromycin; Dox, Doxycycline; Chlor, Chloramphenicol.

1186

1187 **References**

1188 Alteri, C.J., Himpel, S.D., and Mobley, H.L. (2015). Preferential use of central metabolism in vivo
1189 reveals a nutritional basis for polymicrobial infection. *PLoS Pathog* 11, e1004601.

- 1190 Amabebe, E., and Anumba, D.O.C. (2018). The Vaginal Microenvironment: The Physiologic Role
1191 of Lactobacilli. *Front Med (Lausanne)* 5, 181.
- 1192 Ammitzboll, N., Bau, B.P.J., Bundgaard-Nielsen, C., Villadsen, A.B., Jensen, A.M., Leutscher,
1193 P.D.C., Glavind, K., Hagstrom, S., Arenholt, L.T.S., and Sorensen, S. (2021). Pre- and
1194 postmenopausal women have different core urinary microbiota. *Sci Rep* 11, 2212.
- 1195 Andrews, S. (2015). FastQC: a quality control tool for high throughput sequence data.
- 1196 Anglim, B., Phillips, C., Shynlova, O., and Alarab, M. (2021). The effect of local estrogen therapy
1197 on the urinary microbiome composition of postmenopausal women with and without recurrent
1198 urinary tract infections. *Int Urogynecol J*.
- 1199 Arsic, B., Barber, J., Cikos, A., Mladenovic, M., Stankovic, N., and Novak, P. (2018). 16-
1200 membered macrolide antibiotics: a review. *Int J Antimicrob Agents* 51, 283-298.
- 1201 Atassi, F., Pho Viet Ahn, D.L., and Lievin-Le Moal, V. (2019). Diverse Expression of Antimicrobial
1202 Activities Against Bacterial Vaginosis and Urinary Tract Infection Pathogens by Cervicovaginal
1203 Microbiota Strains of *Lactobacillus gasseri* and *Lactobacillus crispatus*. *Front Microbiol* 10, 2900.
- 1204 Barraud, O., Ravry, C., Francois, B., Daix, T., Ploy, M.C., and Vignon, P. (2019). Shotgun
1205 metagenomics for microbiome and resistome detection in septic patients with urinary tract
1206 infections. *Int J Antimicrob Agents*.
- 1207 Bartlett, A.T.M., and White, P.J. (1985). Species of *Bacillus* That Make a Vegetative
1208 Peptidoglycan Containing Lysine Lack Diaminopimelate Epimerase but Have Diaminopimelate
1209 Dehydrogenase. *Microbiology* 131, 2145-2152.
- 1210 Bradshaw, C.S., Tabrizi, S.N., Fairley, C.K., Morton, A.N., Rudland, E., and Garland, S.M. (2006).
1211 The association of *Atopobium vaginae* and *Gardnerella vaginalis* with bacterial vaginosis and
1212 recurrence after oral metronidazole therapy. *J Infect Dis* 194, 828-836.
- 1213 Brubaker, L., and Wolfe, A.J. (2017). The female urinary microbiota, urinary health and common
1214 urinary disorders. *Ann Transl Med* 5, 34.
- 1215 Bucevic Popovic, V., Situm, M., Chow, C.T., Chan, L.S., Roje, B., and Terzic, J. (2018). The
1216 urinary microbiome associated with bladder cancer. *Sci Rep* 8, 12157.
- 1217 Caspi, R., Billington, R., Fulcher, C.A., Keseler, I.M., Kothari, A., Krummenacker, M.,
1218 Latendresse, M., Midford, P.E., Ong, Q., Ong, W.K., *et al.* (2018). The MetaCyc database of
1219 metabolic pathways and enzymes. *Nucleic Acids Res* 46, D633-D639.
- 1220 Correia, S., Poeta, P., Hebraud, M., Capelo, J.L., and Igrejas, G. (2017). Mechanisms of
1221 quinolone action and resistance: where do we stand? *J Med Microbiol* 66, 551-559.
- 1222 Daniel S. C. Butler, A.S., Ann E. Stapleton (2016). Cytoprotective Effect of *Lactobacillus crispatus*
1223 CTV-05 against Uropathogenic *E. coli*. *Pathogens* 5(1).
- 1224 De Nisco, N.J., Neugent, M., Mull, J., Chen, L., Kuprasertkul, A., de Souza Santos, M., Palmer,
1225 K.L., Zimmern, P., and Orth, K. (2019). Direct Detection of Tissue-Resident Bacteria and Chronic

- 1226 Inflammation in the Bladder Wall of Postmenopausal Women with Recurrent Urinary Tract
1227 Infection. *J Mol Biol* 431, 4368-4379.
- 1228 Diop, K., Diop, A., Michelle, C., Richez, M., Rathored, J., Bretelle, F., Fournier, P.E., and Fenollar,
1229 F. (2019). Description of three new *Peptoniphilus* species cultured in the vaginal fluid of a woman
1230 diagnosed with bacterial vaginosis: *Peptoniphilus pacaensis* sp. nov., *Peptoniphilus raoultii* sp.
1231 nov., and *Peptoniphilus vaginalis* sp. nov. *Microbiologyopen* 8, e00661.
- 1232 Edwards, V.L., Smith, S.B., McComb, E.J., Tamarelle, J., Ma, B., Humphrys, M.S., Gajer, P.,
1233 Gwilliam, K., Schaefer, A.M., Lai, S.K., *et al.* (2019). The Cervicovaginal Microbiota-Host
1234 Interaction Modulates *Chlamydia trachomatis* Infection. *MBio* 10.
- 1235 Fait, T. (2019). Menopause hormone therapy: latest developments and clinical practice. *Drugs*
1236 *Context* 8, 212551.
- 1237 Faust, K., Sathirapongsasuti, J.F., Izard, J., Segata, N., Gevers, D., Raes, J., and Huttenhower,
1238 C. (2012). Microbial co-occurrence relationships in the human microbiome. *PLoS Comput Biol* 8,
1239 e1002606.
- 1240 Flores-Mireles, A.L., Walker, J.N., Caparon, M., and Hultgren, S.J. (2015). Urinary tract infections:
1241 epidemiology, mechanisms of infection and treatment options. *Nat Rev Microbiol* 13, 269-284.
- 1242 Fouts, D.E., Pieper, R., Szpakowski, S., Pohl, H., Knoblach, S., Suh, M.J., Huang, S.T.,
1243 Ljungberg, I., Sprague, B.M., Lucas, S.K., *et al.* (2012). Integrated next-generation sequencing of
1244 16S rDNA and metaproteomics differentiate the healthy urine microbiome from asymptomatic
1245 bacteriuria in neuropathic bladder associated with spinal cord injury. *J Transl Med* 10, 174.
- 1246 Franzosa, E.A., McIver, L.J., Rahnvard, G., Thompson, L.R., Schirmer, M., Weingart, G., Lipson,
1247 K.S., Knight, R., Caporaso, J.G., Segata, N., *et al.* (2018). Species-level functional profiling of
1248 metagenomes and metatranscriptomes. *Nat Methods* 15, 962-968.
- 1249 Gaitonde, S., Malik, R.D., and Zimmern, P.E. (2019). Financial Burden of Recurrent Urinary Tract
1250 Infections in Women: A Time-driven Activity-based Cost Analysis. *Urology* 128, 47-54.
- 1251 Gilbert, N.M., Foster, L.R., Cao, B., Yin, Y., Mysorekar, I.U., and Lewis, A.L. (2021). *Gardnerella*
1252 *vaginalis* promotes group B *Streptococcus* vaginal colonization, enabling ascending
1253 uteroplacental infection in pregnant mice. *Am J Obstet Gynecol* 224, 530 e531-530 e517.
- 1254 Glover, M., Moreira, C.G., Sperandio, V., and Zimmern, P. (2014). Recurrent urinary tract
1255 infections in healthy and nonpregnant women. *Urol Sci* 25, 1-8.
- 1256 Hardy, L., Jespers, V., Abdellati, S., De Baetselier, I., Mwambarangwe, L., Musengamana, V.,
1257 van de Wijgert, J., Vaneechoutte, M., and Crucitti, T. (2016). A fruitful alliance: the synergy
1258 between *Atopobium vaginae* and *Gardnerella vaginalis* in bacterial vaginosis-associated biofilm.
1259 *Sex Transm Infect* 92, 487-491.
- 1260 Hardy, L., Jespers, V., Dahchour, N., Mwambarangwe, L., Musengamana, V., Vaneechoutte, M.,
1261 and Crucitti, T. (2015). Unravelling the Bacterial Vaginosis-Associated Biofilm: A Multiplex
1262 *Gardnerella vaginalis* and *Atopobium vaginae* Fluorescence In Situ Hybridization Assay Using
1263 Peptide Nucleic Acid Probes. *PLoS One* 10, e0136658.

- 1264 Hilt, E.E., McKinley, K., Pearce, M.M., Rosenfeld, A.B., Zilliox, M.J., Mueller, E.R., Brubaker, L.,
1265 Gai, X., Wolfe, A.J., and Schreckenberger, P.C. (2014). Urine is not sterile: use of enhanced urine
1266 culture techniques to detect resident bacterial flora in the adult female bladder. *J Clin Microbiol*
1267 *52*, 871-876.
- 1268 Hudzicki, J. (2009). Kirby-Bauer disk diffusion susceptibility test protocol.
- 1269 Human Microbiome Project, C. (2012). Structure, function and diversity of the healthy human
1270 microbiome. *Nature* *486*, 207-214.
- 1271 Huttenhower, C. KneadData.
- 1272 Ikaheimo, R., Siitonen, A., Heiskanen, T., Karkkainen, U., Kuosmanen, P., Lipponen, P., and
1273 Makela, P.H. (1996). Recurrence of urinary tract infection in a primary care setting: analysis of a
1274 1-year follow-up of 179 women. *Clin Infect Dis* *22*, 91-99.
- 1275 Jeffreys, H. (1946). An invariant form for the prior probability in estimation problems. *Proc R Soc*
1276 *Lond A Math Phys Sci* *186*, 453-461.
- 1277 Jaspers, V., van de Wijgert, J., Cools, P., Verhelst, R., Verstraelen, H., Delany-Moretlwe, S.,
1278 Mwaura, M., Ndayisaba, G.F., Mandaliya, K., Menten, J., *et al.* (2015). The significance of
1279 *Lactobacillus crispatus* and *L. vaginalis* for vaginal health and the negative effect of recent sex: a
1280 cross-sectional descriptive study across groups of African women. *BMC Infect Dis* *15*, 115.
- 1281 Jhang, J.F., and Kuo, H.C. (2017). Recent advances in recurrent urinary tract infection from
1282 pathogenesis and biomarkers to prevention. *Ci Ji Yi Xue Za Zhi* *29*, 131-137.
- 1283 Karstens, L., Asquith, M., Caruso, V., Rosenbaum, J.T., Fair, D.A., Braun, J., Gregory, W.T.,
1284 Nardos, R., and McWeeney, S.K. (2018). Community profiling of the urinary microbiota:
1285 considerations for low-biomass samples. *Nat Rev Urol* *15*, 735-749.
- 1286 Karstens, L., Asquith, M., Davin, S., Stauffer, P., Fair, D., Gregory, W.T., Rosenbaum, J.T.,
1287 McWeeney, S.K., and Nardos, R. (2016). Does the Urinary Microbiome Play a Role in Urgency
1288 Urinary Incontinence and Its Severity? *Front Cell Infect Microbiol* *6*, 78.
- 1289 Keogh, D., Tay, W.H., Ho, Y.Y., Dale, J.L., Chen, S., Umashankar, S., Williams, R.B.H., Chen,
1290 S.L., Dunny, G.M., and Kline, K.A. (2016). Enterococcal Metabolite Cues Facilitate Interspecies
1291 Niche Modulation and Polymicrobial Infection. *Cell Host Microbe* *20*, 493-503.
- 1292 Kõljalg, S., Truusalu, K., Vainumäe, I., Stsepetova, J., Sepp, E., and Mikelsaar, M. (2009).
1293 Persistence of *Escherichia coli* Clones and Phenotypic and Genotypic Antibiotic
1294 Resistance in Recurrent Urinary Tract Infections in Childhood. *Journal of Clinical Microbiology* *47*,
1295 99-105.
- 1296 Krueger, F. Trim Galore!
- 1297 Lewis, D.A., Brown, R., Williams, J., White, P., Jacobson, S.K., Marchesi, J.R., and Drake, M.J.
1298 (2013). The human urinary microbiome; bacterial DNA in voided urine of asymptomatic adults.
1299 *Front Cell Infect Microbiol* *3*, 41.

- 1300 Li, Q., Jiang, S., Koh, A.Y., Xiao, G., and Zhan, X. (2019). Bayesian Modeling of Microbiome Data
1301 for Differential Abundance Analysis, pp. arXiv:1902.08741.
- 1302 Lobo, R.A. (2017). Hormone-replacement therapy: current thinking. *Nat Rev Endocrinol* 13, 220-
1303 231.
- 1304 Malik, R.D., Wu, Y.R., Christie, A.L., Alhalabi, F., and Zimmern, P.E. (2018a). Impact of Allergy
1305 and Resistance on Antibiotic Selection for Recurrent Urinary Tract Infections in Older Women.
1306 *Urology* 113, 26-33.
- 1307 Malik, R.D., Wu, Y.R., and Zimmern, P.E. (2018b). Definition of Recurrent Urinary Tract Infections
1308 in Women: Which One to Adopt? *Female Pelvic Med Reconstr Surg* 24, 424-429.
- 1309 Marrazzo, J.M., Thomas, K.K., Fiedler, T.L., Ringwood, K., and Fredricks, D.N. (2008).
1310 Relationship of specific vaginal bacteria and bacterial vaginosis treatment failure in women who
1311 have sex with women. *Ann Intern Med* 149, 20-28.
- 1312 McMurdie, P.J., and Holmes, S. (2013). phyloseq: an R package for reproducible interactive
1313 analysis and graphics of microbiome census data. *PLoS One* 8, e61217.
- 1314 Moustafa, A., Li, W., Singh, H., Moncera, K.J., Torralba, M.G., Yu, Y., Manuel, O., Biggs, W.,
1315 Venter, J.C., Nelson, K.E., *et al.* (2018). Microbial metagenome of urinary tract infection. *Sci Rep*
1316 8, 4333.
- 1317 Neugent, M.L., Hulyalkar, N.V., Nguyen, V.H., Zimmern, P.E., and De Nisco, N.J. (2020).
1318 Advances in Understanding the Human Urinary Microbiome and Its Potential Role in Urinary Tract
1319 Infection. *mBio* 11.
- 1320 Onderdonk, A.B., Delaney, M.L., and Fichorova, R.N. (2016). The Human Microbiome during
1321 Bacterial Vaginosis. *Clin Microbiol Rev* 29, 223-238.
- 1322 Pavoine, S., Dufour, A.B., and Chessel, D. (2004). From dissimilarities among species to
1323 dissimilarities among communities: a double principal coordinate analysis. *J Theor Biol* 228, 523-
1324 537.
- 1325 Pearce, M.M., Hilt, E.E., Rosenfeld, A.B., Zilliox, M.J., Thomas-White, K., Fok, C., Kliethermes,
1326 S., Schreckenberger, P.C., Brubaker, L., Gai, X., *et al.* (2014). The female urinary microbiome: a
1327 comparison of women with and without urgency urinary incontinence. *MBio* 5, e01283-01214.
- 1328 Price, T.K., Dune, T., Hilt, E.E., Thomas-White, K.J., Kliethermes, S., Brincat, C., Brubaker, L.,
1329 Wolfe, A.J., Mueller, E.R., and Schreckenberger, P.C. (2016). The Clinical Urine Culture:
1330 Enhanced Techniques Improve Detection of Clinically Relevant Microorganisms. *J Clin Microbiol*
1331 54, 1216-1222.
- 1332 Price, T.K., Hilt, E.E., Thomas-White, K., Mueller, E.R., Wolfe, A.J., and Brubaker, L. (2019). The
1333 urobiome of continent adult women: a cross-sectional study. *BJOG*.
- 1334 Quince, C., Walker, A.W., Simpson, J.T., Loman, N.J., and Segata, N. (2017). Shotgun
1335 metagenomics, from sampling to analysis. *Nat Biotechnol* 35, 833-844.

- 1336 Raftogianis, R., Creveling, C., Weinshilboum, R., and Weisz, J. (2000). Estrogen metabolism by
1337 conjugation. *J Natl Cancer Inst Monogr*, 113-124.
- 1338 Ravel, J., and Brotman, R.M. (2016). Translating the vaginal microbiome: gaps and challenges.
1339 *Genome Med* 8, 35.
- 1340 Ravel, J., Gajer, P., Abdo, Z., Schneider, G.M., Koenig, S.S., McCulle, S.L., Karlebach, S., Gorle,
1341 R., Russell, J., Tacket, C.O., *et al.* (2011). Vaginal microbiome of reproductive-age women. *Proc*
1342 *Natl Acad Sci U S A* 108 *Suppl 1*, 4680-4687.
- 1343 Rowe, W.P.M., and Winn, M.D. (2018). Indexed variation graphs for efficient and accurate
1344 resistome profiling. *Bioinformatics* 34, 3601-3608.
- 1345 Salter, S.J., Cox, M.J., Turek, E.M., Calus, S.T., Cookson, W.O., Moffatt, M.F., Turner, P., Parkhill,
1346 J., Loman, N.J., and Walker, A.W. (2014). Reagent and laboratory contamination can critically
1347 impact sequence-based microbiome analyses. *BMC Biol* 12, 87.
- 1348 Segata, N., Izard, J., Waldron, L., Gevers, D., Miropolsky, L., Garrett, W.S., and Huttenhower, C.
1349 (2011). Metagenomic biomarker discovery and explanation. *Genome Biol* 12, R60.
- 1350 Segata, N., Waldron, L., Ballarini, A., Narasimhan, V., Jousson, O., and Huttenhower, C. (2012).
1351 Metagenomic microbial community profiling using unique clade-specific marker genes. *Nat*
1352 *Methods* 9, 811-814.
- 1353 Siddiqui, H., Nederbragt, A.J., Lagesen, K., Jeansson, S.L., and Jakobsen, K.S. (2011).
1354 Assessing diversity of the female urine microbiota by high throughput sequencing of 16S rDNA
1355 amplicons. *BMC Microbiol* 11, 244.
- 1356 Stamm, W.E., and Norrby, S.R. (2001). Urinary tract infections: disease panorama and
1357 challenges. *J Infect Dis* 183 *Suppl 1*, S1-4.
- 1358 Stapleton, A.E., Au-Yeung, M., Hooton, T.M., Fredricks, D.N., Roberts, P.L., Czaja, C.A., Yarova-
1359 Yarovaya, Y., Fiedler, T., Cox, M., and Stamm, W.E. (2011). Randomized, placebo-controlled
1360 phase 2 trial of a *Lactobacillus crispatus* probiotic given intravaginally for prevention of recurrent
1361 urinary tract infection. *Clin Infect Dis* 52, 1212-1217.
- 1362 Suzek, B.E., Wang, Y., Huang, H., McGarvey, P.B., Wu, C.H., and UniProt, C. (2015). UniRef
1363 clusters: a comprehensive and scalable alternative for improving sequence similarity searches.
1364 *Bioinformatics* 31, 926-932.
- 1365 Theriot, C.M., Koenigsnecht, M.J., Carlson, P.E., Jr., Hatton, G.E., Nelson, A.M., Li, B.,
1366 Huffnagle, G.B., J, Z.L., and Young, V.B. (2014). Antibiotic-induced shifts in the mouse gut
1367 microbiome and metabolome increase susceptibility to *Clostridium difficile* infection. *Nat Commun*
1368 5, 3114.
- 1369 Thomas-White, K., Forster, S.C., Kumar, N., Van Kuiken, M., Putonti, C., Stares, M.D., Hilt, E.E.,
1370 Price, T.K., Wolfe, A.J., and Lawley, T.D. (2018). Culturing of female bladder bacteria reveals an
1371 interconnected urogenital microbiota. *Nat Commun* 9, 1557.
- 1372 Thomas-White, K., Taege, S., Limeira, R., Brincat, C., Joyce, C., Hilt, E.E., Mac-Daniel, L., Radek,
1373 K.A., Brubaker, L., Mueller, E.R., *et al.* (2020). Vaginal estrogen therapy is associated with

- 1374 increased *Lactobacillus* in the urine of postmenopausal women with overactive bladder
1375 symptoms. *Am J Obstet Gynecol* 223, 727 e721-727 e711.
- 1376 Thomas-White, K.J., Kliethermes, S., Rickey, L., Lukacz, E.S., Richter, H.E., Moalli, P., Zimmern,
1377 P., Norton, P., Kusek, J.W., Wolfe, A.J., *et al.* (2017). Evaluation of the urinary microbiota of
1378 women with uncomplicated stress urinary incontinence. *Am J Obstet Gynecol* 216, 55 e51-55
1379 e16.
- 1380 Vaishnava, S., Yamamoto, M., Severson, K.M., Ruhn, K.A., Yu, X., Koren, O., Ley, R., Wakeland,
1381 E.K., and Hooper, L.V. (2011). The antibacterial lectin RegIII γ promotes the spatial
1382 segregation of microbiota and host in the intestine. *Science* 334, 255-258.
- 1383 van der Berg, C.L., Venter, G., van der Westhuizen, F.H., and Erasmus, E. (2020). Data on the
1384 optimisation of a solid phase extraction method for fractionating estrogen metabolites from small
1385 urine volumes. *Data Brief* 29, 105222.
- 1386 Vaughan, M.H., Mao, J., Karstens, L.A., Ma, L., Amundsen, C.L., Schmader, K.E., and Siddiqui,
1387 N.Y. (2021). The Urinary Microbiome in Postmenopausal Women with Recurrent Urinary Tract
1388 Infections. *J Urol* 206, 1222-1231.
- 1389 Waller, T.A., Pantin, S.A.L., Yenior, A.L., and Pujalte, G.G.A. (2018). Urinary Tract Infection
1390 Antibiotic Resistance in the United States. *Prim Care* 45, 455-466.
- 1391 Whittaker, P.G., Morgan, M.R.A., Dean, P.D.G., Cameron, E.H.D., and Lind, T. (1980). SERUM
1392 EQUILIN, ŒSTRONE, AND ŒSTRADIOL LEVELS IN POSTMENOPAUSAL WOMEN
1393 RECEIVING CONJUGATED EQUINE ŒSTROGENS ('PREMARIN'). *The Lancet* 315, 14-16.
- 1394 Wingett, S.W., and Andrews, S. (2018). FastQ Screen: A tool for multi-genome mapping and
1395 quality control. *F1000Res* 7, 1338.
- 1396 Wolfe, A.J., Toh, E., Shibata, N., Rong, R., Kenton, K., Fitzgerald, M., Mueller, E.R.,
1397 Schreckenberger, P., Dong, Q., Nelson, D.E., *et al.* (2012). Evidence of uncultivated bacteria in
1398 the adult female bladder. *J Clin Microbiol* 50, 1376-1383.
1399

Table 1

Cohort	N-Value	Age \pm SD	BMI \pm SD	Urine pH \pm SD
No UTI History	25	71.3 \pm 9.41	25.4 \pm 4.37	6.4 \pm 1.06
rUTI Remission	25	70.4 \pm 8.25	24.6 \pm 4.18	6.0 \pm 1.08
rUTI Relapse	25	75.7 \pm 7.62	26.6 \pm 4.30	5.64 \pm 0.88

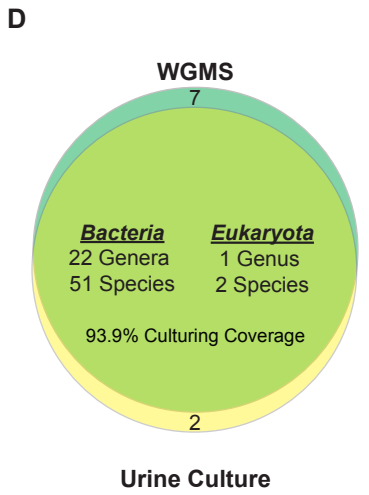
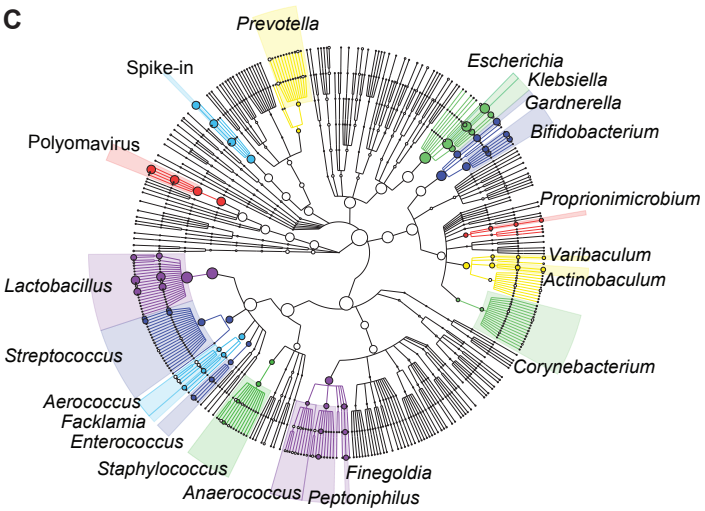
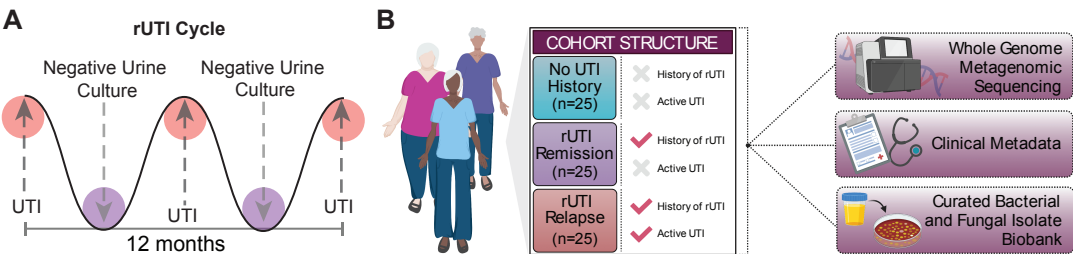
Figure 1

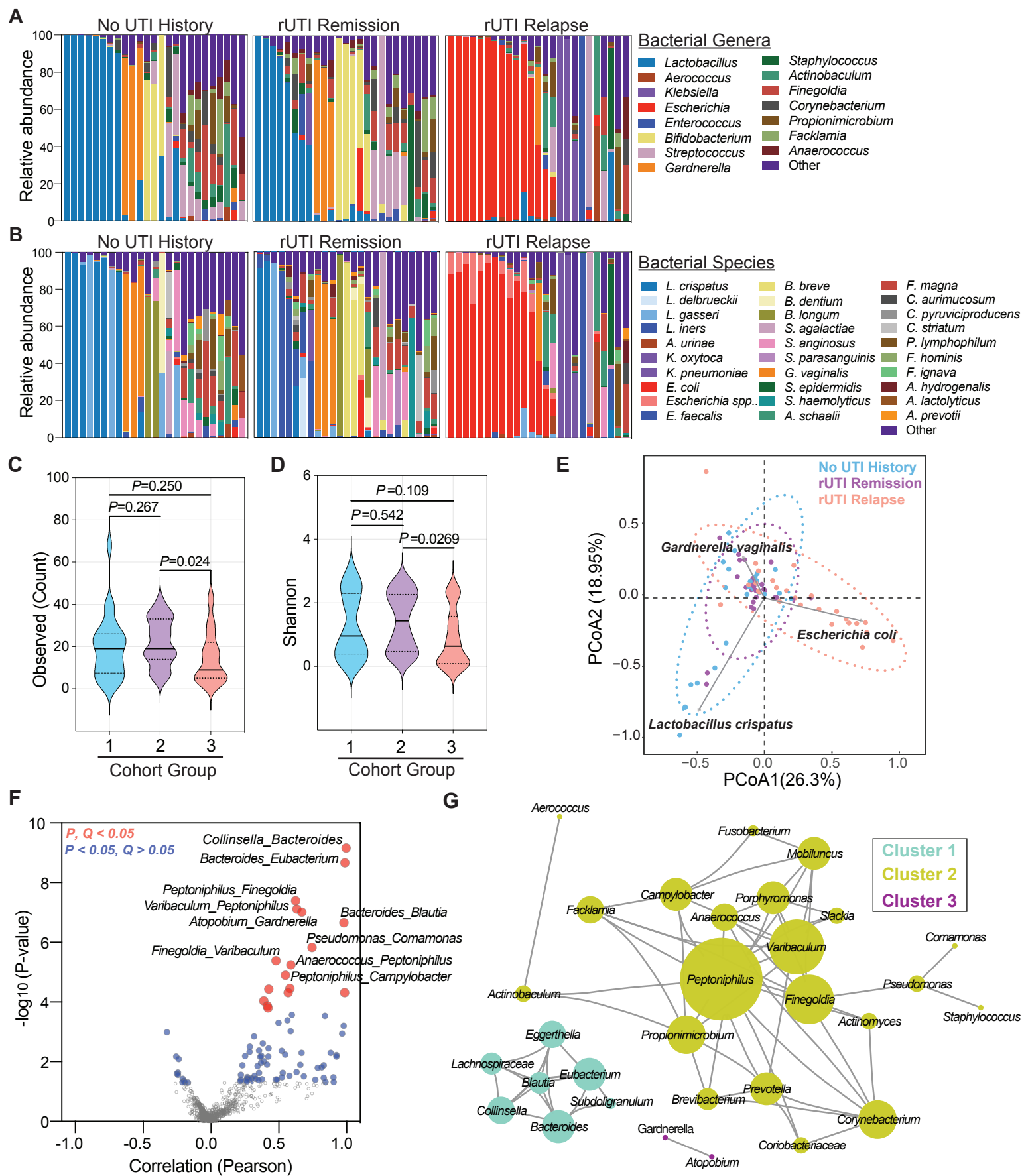
Figure 2

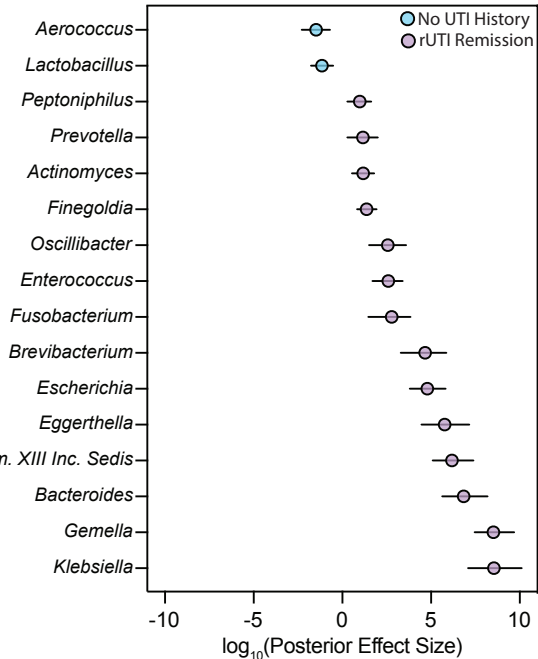
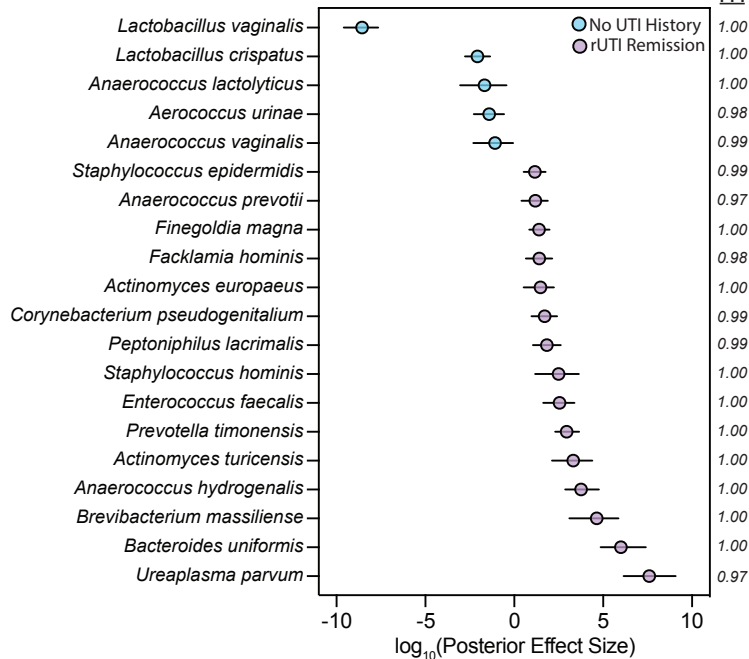
Figure 3**A****PPI****B****PPI**

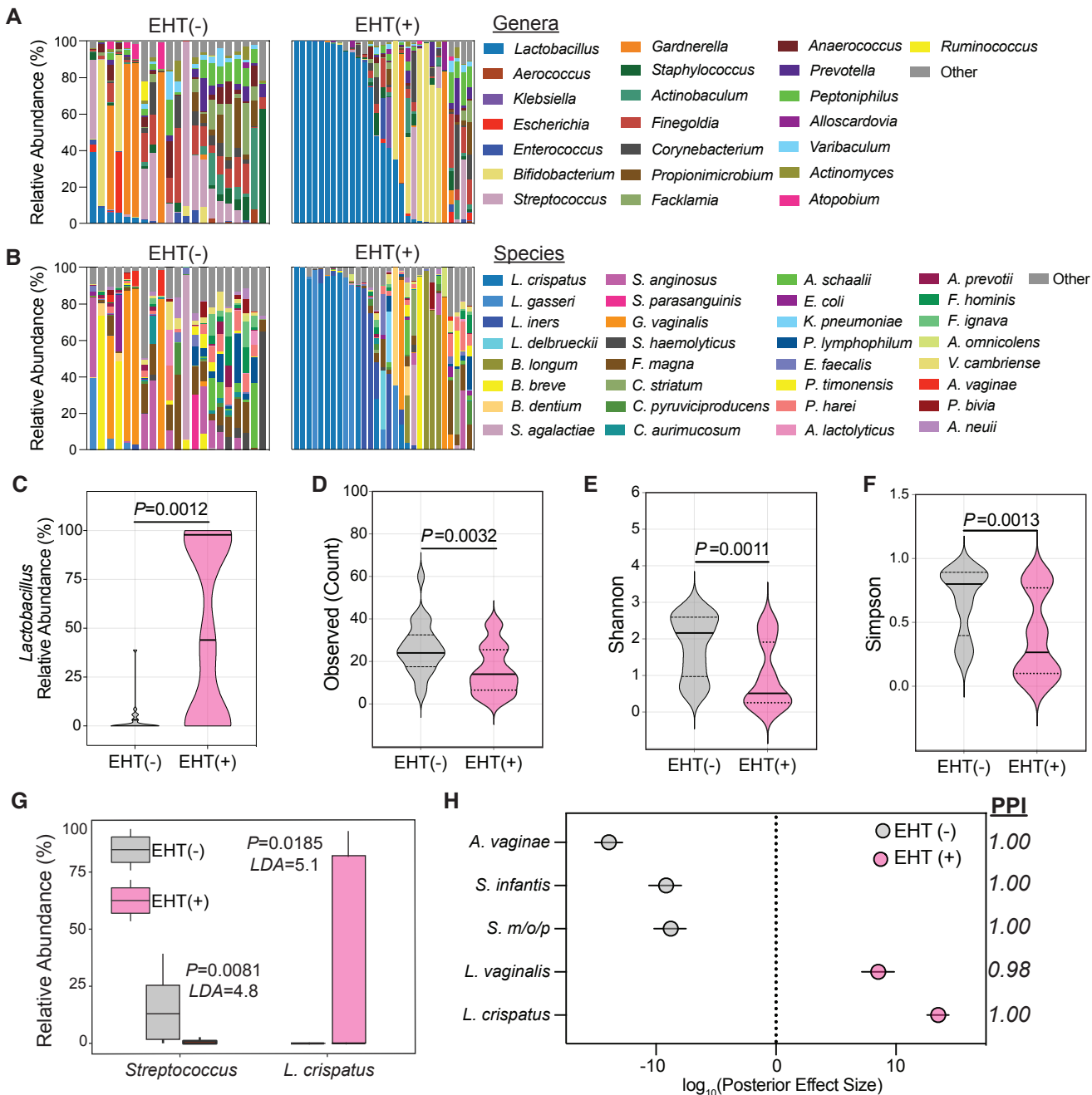
Figure 4

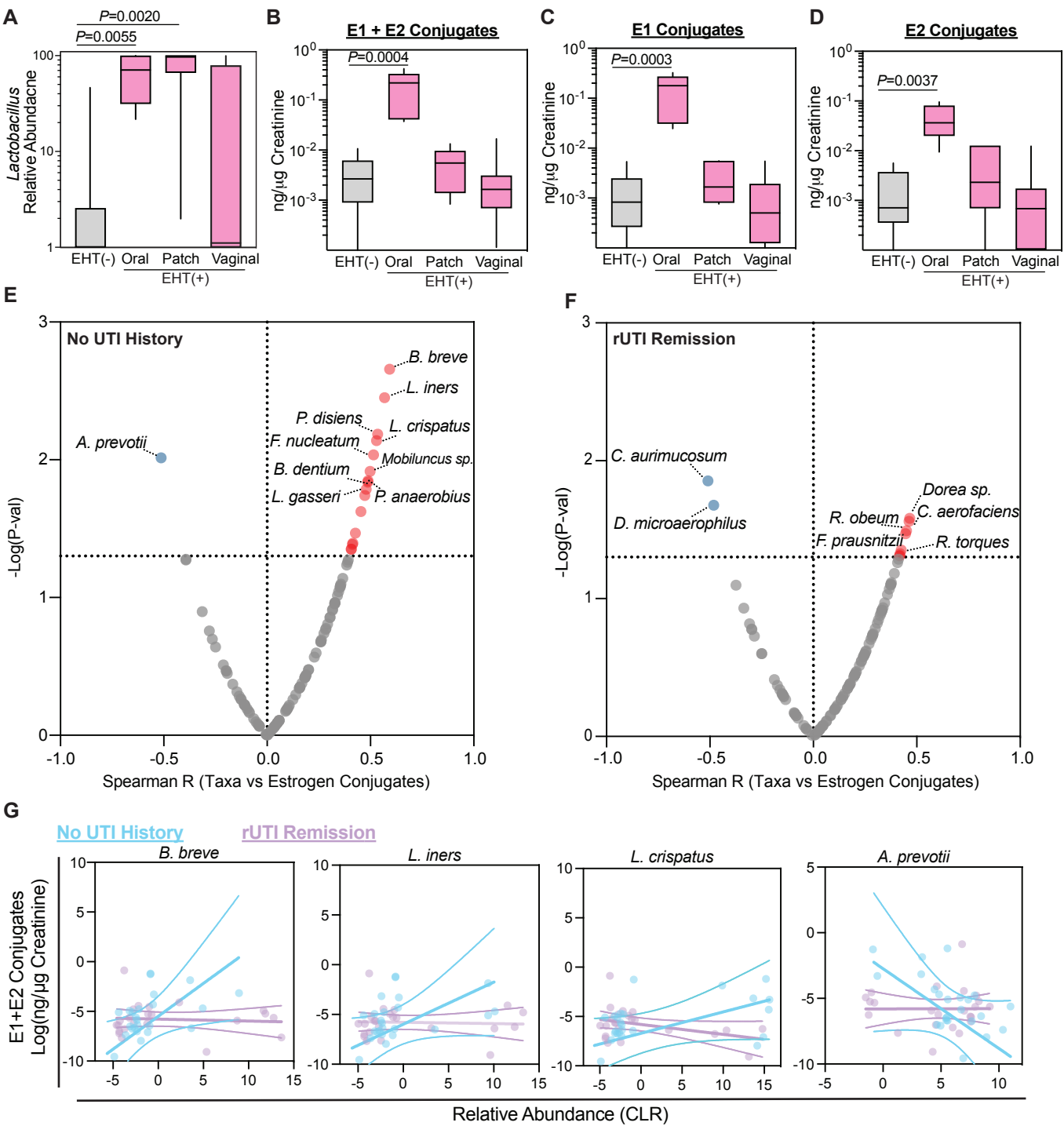
Figure 5

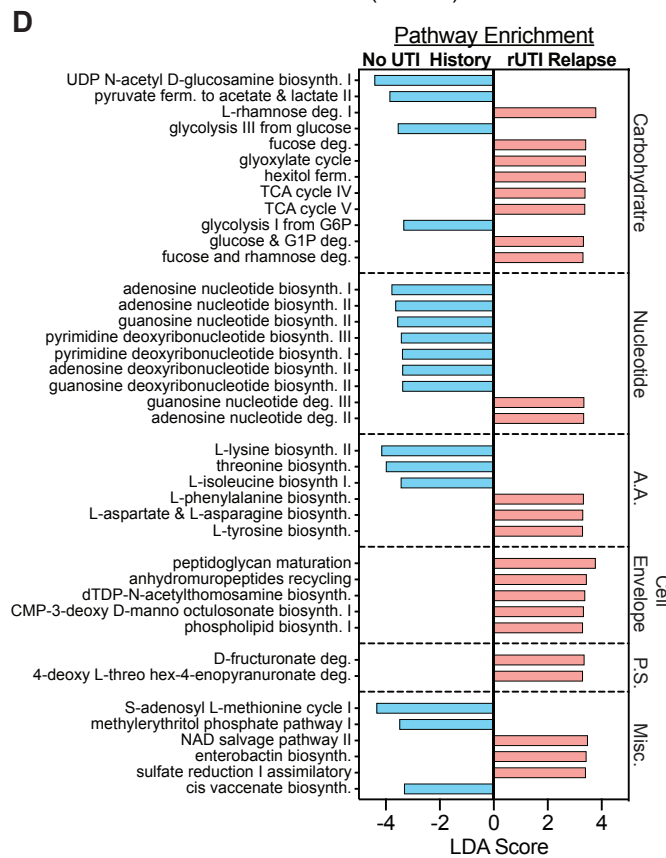
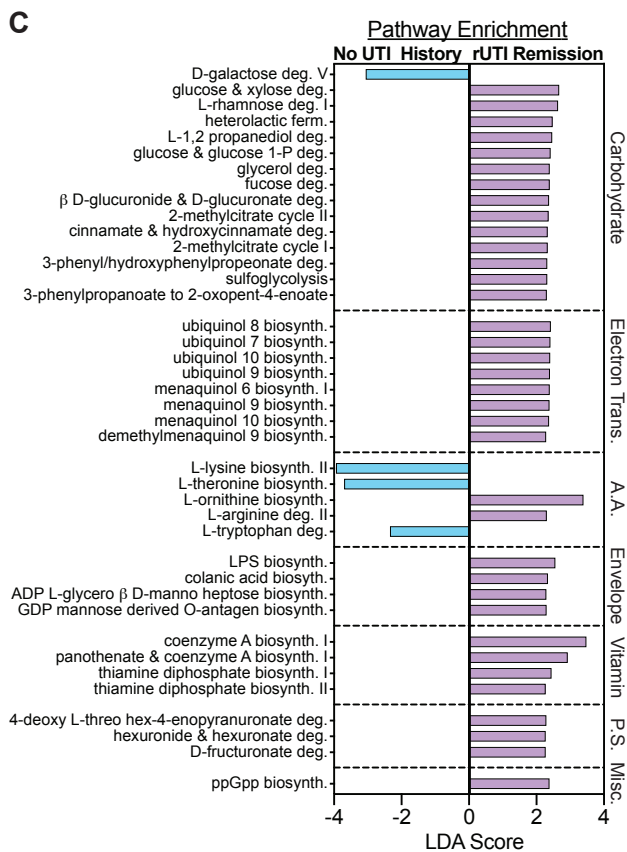
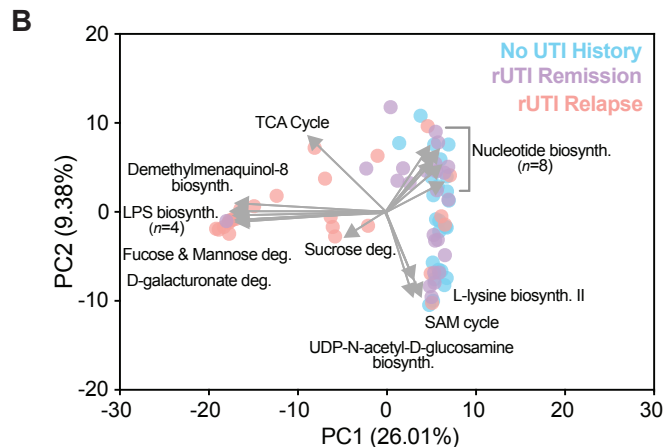
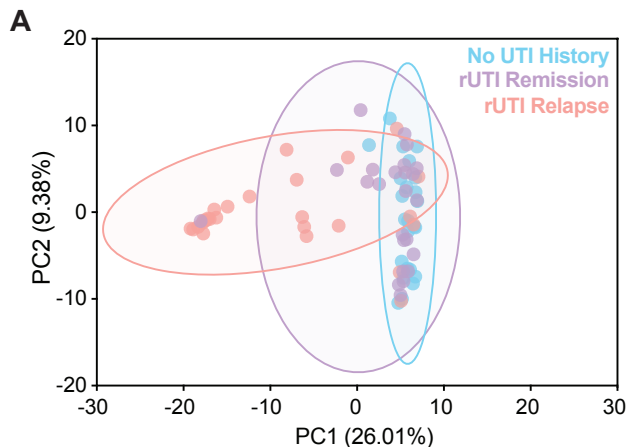
Figure 6

Figure 7

